

1 **Nocturnal Atmospheric Synergistic Oxidation Reduces the Formation of Low-volatility**
2 **Organic Compounds from Biogenic Emissions**

3 Han Zang¹, Zekun Luo¹, Chenxi Li¹, Ziyue Li¹, Dandan Huang^{2,*}, Yue Zhao^{1,*}

4

5 ¹School of Environmental Science and Engineering, Shanghai Jiao Tong University, Shanghai,
6 200240, China

7 ²Shanghai Academy of Environmental Sciences, Shanghai, 200233, China

8 *Correspondence: Yue Zhao (yuezhao20@sjtu.edu.cn); Dandan Huang (huangdd@saes.sh.cn);

9

10 **Abstract**

11 Volatile organic compounds (VOCs) are often subject to synergistic oxidation by different oxidants
12 in the atmosphere. However, the exact synergistic oxidation mechanism of atmospheric VOCs and
13 its role in particle formation remain poorly understood. In particular, the reaction kinetics of the key
14 reactive intermediates, organic peroxy radicals (RO₂), during synergistic oxidation is rarely studied.
15 Here, we conducted a combined experimental and kinetic modelling study of the nocturnal
16 synergistic oxidation of α -pinene (the most abundant monoterpene) by O₃ and NO₃ radicals as well
17 as its influences on the formation of highly oxygenated organic molecules (HOMs) and particles.
18 We find that in the synergistic O₃ + NO₃ regime, where OH radicals are abundantly formed via
19 decomposition of ozonolysis-derived Criegee intermediates, the production of C_xH_yO_z-HOMs is
20 substantially suppressed compared to that in the O₃-only regime, mainly because of the depletion of
21 of α -pinene RO₂ derived from ozonolysis and OH oxidation by those arising from NO₃ oxidation
22 via cross reactions. Measurement-model comparisons further reveal that the cross-reaction rate
23 constants of NO₃-derived RO₂ with O₃-derived RO₂ are on average 10 – 100 times larger than those
24 of NO₃-derived RO₂ with OH-derived RO₂. Despite a strong production of organic nitrates in the
25 synergistic oxidation regime, the substantial decrease of C_xH_yO_z-HOM formation leads to a
26 significant reduction in ultralow- and extremely low-volatility organic compounds, which
27 significantly inhibits the formation of new particles. This work provides valuable mechanistic and
28 quantitative insights into the nocturnal synergistic oxidation chemistry of biogenic emissions and
29 will help to better understand the formation of low-volatility organic compounds and particles in
30 the atmosphere.

31

32 **1. Introduction**

33 The Earth's atmosphere is a complex oxidizing environment in which multiple oxidants coexist.
34 During the nighttime, NO₃ radicals (generated by the reaction of NO₂ and O₃) and O₃ contribute
35 significantly to the oxidation of volatile organic compounds (VOCs) (Huang et al., 2019), while
36 during the daytime, the fast photolysis of NO₃ radicals and rapid photochemical formation of OH
37 radicals and O₃ make the latter two the major oxidants for VOCs (Zhang et al., 2018). Therefore,
38 the degradation of ambient VOCs is subject to concurrent oxidation by different oxidants. Gas-phase
39 oxidation of VOCs from biogenic emissions (BVOCs) by these major atmospheric oxidants
40 produces a key type of reactive intermediates, organic peroxy radicals (RO₂), a portion of which can
41 undergo fast autoxidation forming a class of highly oxygenated organic molecules (HOMs) with
42 low volatilities (Jokinen et al., 2014; Mentel et al., 2015; Berndt et al., 2016; Zhao et al., 2018; Iyer
43 et al., 2021; Shen et al., 2022; Ehn et al., 2014). HOMs typically contain six or more oxygen atoms,
44 and plays a key role in the formation of atmospheric new particles and secondary organic aerosol
45 (SOA) (Kirkby et al., 2016; Berndt et al., 2018a; Zhao et al., 2018; Ehn et al., 2014; Bianchi et al.,
46 2019), which have important influences on air quality (Huang et al., 2014), public health (Pye et al.,
47 2021), and Earth's radiative forcing (Shrivastava et al., 2017).

48 Due to the complexity of oxidation mechanisms of BVOCs, previous laboratory studies typically
49 featured only one oxidant and a single SOA precursor (Berndt et al., 2016; Berndt, 2021; Clafin et
50 al., 2018; Iyer et al., 2021; Boyd et al., 2015). However, the synergistic oxidation by different
51 oxidants may significantly alter the fate of RO₂ intermediates, therefore influencing the formation
52 of HOMs and SOA (Bates et al., 2022). Recently, a field study at a boreal forest site in Finland
53 observed a series of nitrate-containing HOM-dimers from the coupled O₃ and NO₃ oxidation of
54 monoterpenes (Zhang et al., 2020). At the same site, Lee et al. (2020) found that the synergistic
55 oxidation of BVOCs by OH radicals and O₃ contributed to the largest fraction of SOA. These studies
56 suggest that the synergistic oxidation of BVOCs by different oxidants plays an important role in the
57 formation of HOMs and SOA in the atmosphere and highlight the needs to investigate the synergistic
58 oxidation mechanisms of BVOCs for a better representation of atmospheric particle formation.

59 Several laboratory studies have attempted to address the role of synergistic oxidation of BVOCs in
60 the formation of new particles and SOA (Kenseth et al., 2018; Inomata, 2021; Liu et al., 2022; Li et

61 al., 2024). Kenseth et al. (2018) identified a suite of dimer esters in flow tube experiments that can
62 be only formed from the OH and O₃ synergistic oxidation of β-pinene. These dimers exhibit
63 extremely low volatility and contributed 5.9 – 25.4% to the total β-pinene SOA. Similarly, Inomata
64 (2021) found that the presence of OH radicals during α-pinene ozonolysis is a key factor for the
65 production of low-volatility organic species and significantly promotes new particle formation
66 (NPF). On the other hand, the addition of O₃ in the monoterpene photooxidation system also
67 significantly increases the SOA mass yield (Liu et al., 2022). In addition, a recent chamber study
68 by Bates et al. (2022) showed that the synergistic oxidation of α-pinene by NO₃ radicals and O₃ can
69 significantly enhance the SOA yield compared to the NO₃ + α-pinene regime, which has nearly 0%
70 SOA yield (Fry et al., 2014; Hallquist et al., 1999; Mutzel et al., 2021), and they revealed that the
71 SOA yield in the NO₃ + O₃ oxidation system largely depends on the RO₂ fates. Most recently, Li et
72 al. (2024) found that during α-pinene ozonolysis, the presence of nitrooxy-RO₂ radicals formed from
73 NO₃ oxidation can significantly suppress the production of ultralow-volatility organic compounds
74 (ULVOCs) and thereby NPF. These laboratory studies together provide growing evidence that
75 synergistic oxidation of BVOCs by different oxidants have profound impacts on atmospheric
76 particle formation. However, the specific synergistic mechanisms of different oxidants and
77 oxidation pathways remain obscure. Although a few studies underscored the importance of the RO₂
78 fates (Bates et al., 2022; Li et al., 2024), the exact interactions between RO₂ species derived from
79 different oxidants are still unclear, and quantitative constraints on the reaction rate of different RO₂
80 species are quite limited.

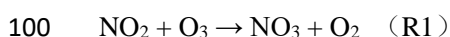
81 Here we conducted an investigation of the synergistic O₃ + NO₃ oxidation of α-pinene, one of the
82 most abundant monoterpenes in the atmosphere, using a combination of laboratory experiments and
83 detailed kinetic modelling, and focusing on the fate of RO₂ intermediates arising from different
84 oxidation pathways. The α-pinene oxidation experiments were conducted in a custom-built flow
85 reactor. The molecular composition of RO₂ species and HOMs in different oxidation regimes was
86 characterized using a chemical ionization atmospheric pressure interface time-of-flight mass
87 spectrometer (CI-APi-ToF) employing a nitrate ion source. The measured distributions of specific
88 RO₂ and HOMs across different oxidation regimes were fitted with a kinetic model using Master
89 Chemical Mechanisms (MCM v3.3.1) updated with recent advances of α-pinene RO₂ chemistry

90 (Wang et al., 2021; Iyer et al., 2021; Shen et al., 2022; Zang et al., 2023), which allows for
91 quantitative constraints on RO₂ kinetics and synergistic oxidation mechanisms. Atmospheric
92 relevance of the experimental results was evaluated by modelling the investigated oxidation
93 chemistry under typical nocturnal atmospheric conditions.

94 **2. Materials and Methods**

95 **2.1 Flow tube experiments**

96 Experiments of α -pinene oxidation in different regimes (i.e., synergistic O₃ + NO₃ oxidation vs. O₃-
97 only) were carried out under room temperature (298 K) and dry (relative humidity < 5%) conditions
98 in a custom-built flow tube reactor (FTR, Figure S1). O₃ and NO₂ were added into a glass tube
99 (Figure S1) to form NO₃ radical and its precursor N₂O₅:



102 O₃ was generated by passing a flow of ultra-high-purity (UHP) O₂ (Shanghai Maytor Special Gas
103 Co., Ltd.) through a quartz tube housing a pen-ray mercury lamp (UV-S2, UVP Inc.) and its
104 concentration was measured by an ozone analyzer (T400, API). NO₂ was obtained from a gas
105 cylinder (15.6 ppm, Shanghai Weichuang Standard Gas Co., Ltd.). The initial NO₂ concentration in
106 the flow tube was ~4.5 ppb. To prevent the titration of NO₃ radicals by NO, all the experiments
107 were performed without the addition of NO. The total air flow in the NO₃ generation glass tube was
108 0.6 L min⁻¹ and 0.4 L min⁻¹ for the gas-phase HOM and SOA formation experiments, respectively.
109 The produced N₂O₅ and NO₃ radicals, as well as the excessive O₃ were added into the FTR to initiate
110 α -pinene oxidation. For the O₃-only experiments, only O₃ was added into FTR.

111 The α -pinene gas was generated by evaporating a defined volume of its liquid (99%, Sigma-Aldrich)
112 into a cleaned and evacuated canister (SilcoCan, RESTEK), and then added into FTR through a
113 movable injector at a flow rate of 22 – 108 mL min⁻¹. The initial concentration of α -pinene in the
114 flow reactor ranged from 100 – 500 ppb. In some experiments, the gas of cyclohexane (~ 100 ppm),
115 which was generated by bubbling a gentle flow of UHP N₂ through its liquid (LC-MS grade, CNW),
116 was added into the flow reactor as a scavenger of OH radicals formed from α -pinene ozonolysis.

117 For experiments characterizing the formation of HOMs, the total air flow in the FTR was 10.8 L

118 min⁻¹ and the residence time was 25 seconds. The short reaction time and the small amount of
119 reacted α -pinene (see Table S1) in these experiments prevented the formation of particles. For the
120 experiments characterizing the formation of SOA particles, a larger FTR was used, with a total air
121 flow of 5 L min⁻¹ and a residence time of 180 seconds. A summary of the conditions including the
122 simulated concentrations of NO₂, N₂O₅ and NO₃ radicals, as well as the concentration of α -pinene
123 oxidized by each oxidant in different experiments are shown in Table S1.

124 The gas-phase RO₂ radicals and closed-shell products were measured using a nitrate-based CI-API-
125 ToF (abbreviated as nitrate-CIMS; Aerodyne Research, Inc.), which has been described in detail
126 previously (Zang et al., 2023). A long ToF-MS with a mass resolution of ~ 10000 Th/Th was used
127 here. The mass spectra within the m/z range of 50-700 were analyzed using the tofTools package
128 developed by Junninen et al. (2010) based on Matlab. The total ion counts (TIC) with values of $(5.9$
129 $- 6.2) \times 10^4$ cps are similar under different reaction conditions. In this study, we assume that the
130 C_xH_yO_z-HOMs derived from ozonolysis and OH oxidation of α -pinene exhibit the same sensitivity
131 in nitrate-CIMS. However, the highly oxygenated organic nitrates may have a significantly lower
132 sensitivity compared to the C_xH_yO_z-HOM counterparts, given that the substitution of -OOH or -OH
133 groups by -ONO₂ group in the molecule would reduce the number of H-bond donors, which is a
134 key factor determining the sensitivity of nitrate-CIMS (Shen et al., 2022; Hyttinen et al., 2015).
135 Recently, Li et al. (2024) used CI-Orbitrap with ammonium or nitrate reagent ions to detect
136 oxygenated organic molecules in the synergistic O₃ + NO₃ regime and found that both the ion
137 intensity of ONs and their signal contribution to the total dimers were much lower when using nitrate
138 as reagent ions.

139 A scanning mobility particle sizer (SMPS, TSI), consisting of an electrostatic classifier (model
140 3082), a condensation particle counter (model 3756), and a long or nano differential mobility
141 analyzer (model 3081 and 3085) with a measurable size range of 4.61 – 156.8 nm or 14.6 – 661.2
142 nm, respectively, was employed to monitor the formation of particles in the flow tube. During the
143 HOM formation experiments, even under conditions with the highest initial α -pinene concentration
144 (500 ppb), only a tiny amount of particles was formed, with mass concentrations of $(6.4 \pm 1.6) \times 10^{-3}$
145 and $(1.0 \pm 0.3) \times 10^{-2}$ $\mu\text{g m}^{-3}$ and number concentrations of 574 ± 138 and 256 ± 68 cm⁻³ in the O₃-
146 only (Exp 5) and O₃ + NO₃ regimes (Exp 11), respectively. These results suggest that the formation

147 of SOA particles in the HOM formation experiments is negligible and would have no significant
148 influence on the fate of RO₂ and closed-shell products.

149 **2.2 Estimation of HOM volatility**

150 A modified composition-activity method was used to estimate the saturation mass concentration
151 (C*) of HOMs in this study according to the approach developed by Li et al. (2016):

$$152 \log_{10}C^* = (n_C^0 - n_C)b_C - n_O b_O - 2 \frac{n_C n_O}{n_C + n_O} b_{CO} - n_N b_N - n_S b_S$$

153 where n_C^0 is the reference carbon number; n_C , n_O , n_N , and n_S are the atom numbers of carbon,
154 oxygen, nitrogen, and sulfur, respectively; b_C , b_O , b_N , and b_S are the contribution of each atom
155 to $\log_{10}C^*$, respectively; b_{CO} is the carbon–oxygen nonideality (Donahue et al., 2011). These b -
156 values were provided by Li et al. (2016).

157 It should be noted that the CHON compounds used in the data set by Li et al. (2016) are mostly
158 amines, amides, and amino acids, and only contain a limited number of organic nitrates (0.07%).
159 Since different types of CHON compounds have very different vapor pressures (Isaacman-Vanwertz
160 and Aumont, 2021), this formula-based approach can be biased to estimate the C* of organic nitrates.
161 Considering that the –ONO₂ and –OH groups have similar impacts on vapor pressure and that the
162 CHON species are predominantly organic nitrates in our study, all –ONO₂ groups are treated as OH
163 groups during the estimation of vapor pressure (Daumit et al., 2013; Isaacman-Vanwertz and
164 Aumont, 2021).

165 Gas-phase HOMs are grouped into five classes based on their $\log_{10}C^*$ (Donahue et al., 2012;
166 Bianchi et al., 2019; Schervish and Donahue, 2020), that is, ULVOCs ($\log_{10}C^* < -8.5$), extremely
167 low-volatility organic compounds (ELVOCs, $-8.5 < \log_{10}C^* < -4.5$), low-volatility organic
168 compounds (LVOCs, $-4.5 < \log_{10}C^* < -0.5$), semi-volatile organic compounds (SVOCs, $-0.5 <$
169 $\log_{10}C^* < 2.5$), and intermediate-volatility organic compounds (IVOCs, $2.5 < \log_{10}C^* < 6.5$).

170 **2.3 Kinetic model simulations**

171 Model simulations of specific RO₂ radicals and closed-shell HOMs formed in different oxidation
172 regimes were performed to constrain the reaction kinetics and mechanisms using the Framework
173 for 0-D Atmospheric Modeling (F0AM v4.1) (Wolfe et al., 2016), which employs MCM v3.3.1

174 (Jenkin et al., 2015). The α -pinene oxidation mechanism was updated with the state-of-the-art
175 knowledge on the chemistry of RO₂ autoxidation and cross reactions forming HOM monomers and
176 dimers, respectively (Zhao et al., 2018; Wang et al., 2021; Iyer et al., 2021; Shen et al., 2022). The
177 detailed updates have been described in our previous study (Zang et al., 2023). In particular, the
178 formation and subsequent reactions of the ring-opened primary C₁₀H₁₅O₄-RO₂, the highly
179 oxygenated acyl RO₂, as well as the C₁₀H₁₅O₂-RO₂ arising from H-abstraction by OH radicals
180 during α -pinene ozonolysis are included in the model according to recent studies (Iyer et al., 2021;
181 Zhao et al., 2022; Zang et al., 2023; Shen et al., 2022).

182 To investigate the synergistic reactions of RO₂ derived from the oxidation of α -pinene by different
183 oxidants, we added the cross reactions of the primary nitrooxy-RO₂ derived from NO₃ oxidation
184 (^{NO₃}RO₂), i.e., C₁₀H₁₆NO₅-RO₂, with RO₂ derived from ozonolysis (^{Cl}RO₂) and OH oxidation
185 (^{OH}RO₂). Recently, Zhao et al. (2018) revealed the bulk rate constant for ^{Cl}RO₂ and ^{OH}RO₂ self/cross
186 reactions to be $2 \times 10^{-12} \text{ cm}^3 \text{ molecule}^{-1} \text{ s}^{-1}$, and Bates et al. (2022) constrained the rate constant for
187 ^{NO₃}RO₂ self/cross reactions to be $1 \times 10^{-13} - 1 \times 10^{-12} \text{ cm}^3 \text{ molecule}^{-1} \text{ s}^{-1}$. In the present study, the
188 default rate constant for ^{NO₃}RO₂ + ^{Cl}RO₂ was set to $2 \times 10^{-12} \text{ cm}^3 \text{ molecule}^{-1} \text{ s}^{-1}$, the same to that for
189 self/cross reactions of ^{Cl}RO₂ and ^{OH}RO₂. The ratio of the cross-reaction rate constant of ^{NO₃}RO₂ +
190 ^{Cl}RO₂ to that of ^{NO₃}RO₂ + ^{OH}RO₂ was tuned to achieve a good measurement-model agreement for
191 the distribution of specific RO₂ and HOMs across different oxidation regimes. Recent studies
192 suggested that the ROOR' dimer formation rates from the highly oxygenated RO₂ are fast (Berndt
193 et al., 2018b; Molteni et al., 2019). As a result, a relatively high dimer formation branching ratio of
194 50% was used for different RO₂ (e.g., ^{Cl}RO₂, ^{OH}RO₂, ^{NO₃}RO₂) in this study. With these default
195 kinetic parameters, the RO₂ bimolecular lifetimes were predicted to be 10.9 – 25.9 s in the O₃-only
196 regime and 8.4 – 11.8 s in the O₃ + NO₃ regime in the HOM formation experiments. Considering
197 that the RO₂ cross-reaction kinetics remain highly uncertain, sensitivity analyses were performed to
198 evaluate their influences on the results in this study (see Section 3.2). Previous studies indicated that
199 the primary ^{NO₃}RO₂ radicals arising from α -pinene are prone to lose the nitrate group and form
200 pinonaldehyde with high volatility (Kurtín et al., 2017; Fry et al., 2014). Therefore, we did not
201 consider the autoxidation of primary ^{NO₃}RO₂ in the model. Considering the presence of NO₂ in the
202 experiments, the reactions of RO₂ + NO₂ \rightleftharpoons ROONO₂ were also included in the model (Zang et al.,

203 2023).

204 3. Results and Discussion

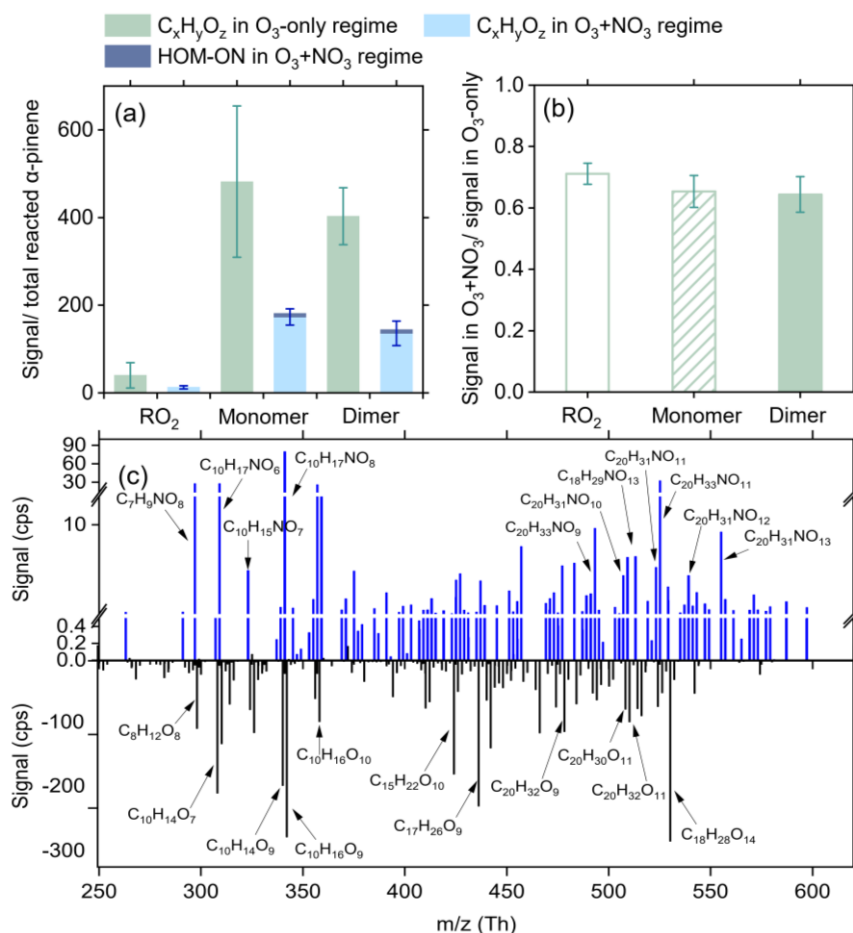
205 3.1 Molecular distribution of RO₂ and HOMs in the synergistic oxidation regime

206 The abundance of gas-phase RO₂ species and HOMs in different oxidation regimes is shown in
207 Figure 1a. The species signals are normalized by the total reacted α -pinene in each regime.
208 Compared to the O₃-only regime, the normalized signals of total RO₂ and HOMs decrease by 62 –
209 68% in the synergistic O₃ + NO₃ regime. Although NO₃ oxidation accounts for a considerable
210 fraction of reacted α -pinene in the synergetic oxidation regime, the signal contributions of HOM-
211 ONs are not significant. This might be due to the low sensitivity of nitrate-CIMS to the ONs formed
212 involving NO₃ oxidation (Section 2.1). Although there remain considerable uncertainties in
213 instrument sensitivities to different compounds, sensitivity analyses suggest that varying the CIMS
214 sensitivities to RO₂ and HOMs by a factor of 10 would not significantly influence their relative
215 distribution across different oxidation regimes (see Section S1 for details).

216 Note that the initial concentrations of α -pinene and O₃ in the two oxidation regimes were the same.
217 In addition, model simulations show that in the synergistic O₃ + NO₃ regime, over 97% of OH
218 radicals react with α -pinene and the depletion of OH by NO₂ is minor (0.2 – 1.3%). Also, NO₃
219 radicals almost entirely (over 98.5%) react with α -pinene and their reaction with RO₂ has negligible
220 influence on the fate of RO₂ (Figure S2). Meanwhile, the depletion of acyl RO₂ by NO₂ only leads
221 to a small reduction (4 – 5% and 7 – 12%, respectively) in total C_xH_yO_z-HOM monomers and dimers
222 in the synergistic regime compared to the O₃-only regime. As a result, the strong reduction in HOM
223 formation due to the presence of NO₃ oxidation is likely mainly due to (i) the fast competitive
224 consumption of α -pinene by NO₃ radicals, which leads to a reduction in the reacted α -pinene by O₃
225 ($\Delta[\alpha\text{-pinene}]_{\text{O}_3}$, Figure S3) and thereby C_xH_yO_z-HOM signals, and (ii) the cross reactions of ^{Cl}RO₂
226 or ^{OH}RO₂ with ^{NO3}RO₂, which suppress the autoxidation and self/cross reactions of ^{Cl}RO₂ and ^{OH}RO₂
227 to form C_xH_yO_z-HOMs.

228 To quantify the contribution of cross reactions of ^{NO3}RO₂ with ^{Cl}RO₂/^{OH}RO₂ to the suppressed
229 formation of C_xH_yO_z-HOMs in the synergistic oxidation regime, C_xH_yO_z-HOM signals shown in
230 Figure 1a are first normalized to $\Delta[\alpha\text{-pinene}]_{\text{O}_3}$ in each oxidation regime and then compared between

231 different oxidation regimes (see Figure 1b). Notably, after excluding the influence of reduced $\Delta[\alpha$ -
 232 pinene]₀₃, the C_xH_yO_z-HOMs signals still drop by 24 – 32% in the O₃ + NO₃ regime compared to
 233 those in the O₃-only regime, indicating a significant contribution of the coupled reactions between
 234 ^{NO3}RO₂ and ^{Cl}RO₂ or ^{OH}RO₂ to suppressed C_xH_yO_z-HOM formation.



235
 236 Figure 1 Distributions of RO₂ and HOMs in the O₃-only and O₃ + NO₃ regimes. (a) Signals of total
 237 RO₂, as well as HOM monomers and dimers normalized by the reacted α -pinene in each oxidation
 238 regime (Exps 1-5, 7-11). (b) Relative changes in the normalized signals of C_xH_yO_z-HOMs in the O₃
 239 + NO₃ regime versus the O₃-only regime. Ion signals are normalized to $\Delta[\alpha$ -pinene]₀₃ in each
 240 oxidation regime to highlight the suppression effect of the synergistic chemistry between ^{NO3}RO₂
 241 and ^{Cl}RO₂ or ^{OH}RO₂ on C_xH_yO_z-HOM formation. (c) Difference mass spectrum between the two
 242 oxidation regimes. The positive and negative peaks indicate the species with enhanced and
 243 decreased formation in the O₃ + NO₃ regime compared to the O₃-only regime, respectively.

244 Figure 1c shows a difference mass spectrum highlighting the changes in species distribution
 245 between the two oxidation regimes. Almost all C_xH_yO_z-HOM species decrease significantly in the
 246 O₃ + NO₃ regime compared to the O₃-only regime. Besides, a large set of HOM-ON species are
 247 formed, despite their relatively low signals. It should be noted that no obvious signals of highly

248 oxygenated NO_3RO_2 ($\text{C}_{10}\text{H}_{16}\text{NO}_x$, $x \geq 6$) were observed by nitrate-CIMS in the $\text{O}_3 + \text{NO}_3$ oxidation
249 system. One possible reason is that nitrate-CIMS exhibits relatively low sensitivity to the organic
250 nitrates. Secondly, the instrument's mass resolution is not high enough to differentiate the mass
251 closure between some of NO_3RO_2 and $\text{C}_x\text{H}_y\text{O}_z$ -HOMs with strong peaks (Table S3), limiting the
252 detection of NO_3RO_2 species. Furthermore, previous studies revealed that the primary NO_3RO_2
253 radicals (i.e., $\text{C}_{10}\text{H}_{16}\text{NO}_5\text{-RO}_2$) in the α -pinene + NO_3 system mainly react to form pinonaldehyde
254 (Kurtén et al., 2017; Perraud et al., 2010). It is likely that only a very small amount of NO_3RO_2 can
255 undergo intramolecular H-shift/ O_2 addition to form highly oxygenated NO_3RO_2 . It should be pointed
256 out that although the primary $\text{C}_{10}\text{H}_{16}\text{NO}_5\text{-RO}_2$ species arising from NO_3 oxidation may not undergo
257 fast autoxidation, they tend to efficiently terminate ClRO_2 and/or OHRO_2 and suppress the formation
258 of $\text{C}_x\text{H}_y\text{O}_z$ -HOMs.

259 As shown in Figure 1c, although several closed-shell monomeric HOM-ONs have been observed in
260 the synergistic oxidation regime, only a few of them exhibit relatively high signals. Among them,
261 $\text{C}_{10}\text{H}_{17}\text{NO}_8$ may be formed by the autoxidation of $\text{C}_{10}\text{H}_{16}\text{NO}_6\text{-RO}_2$ derived from the intramolecular
262 H-shift of primary NO_3RO radicals ($\text{C}_{10}\text{H}_{16}\text{NO}_4\text{-RO}$). In addition, although CI is a soft ionization
263 method, the fragmentation of chemically labile species still occurs during the ionization in nitrate-
264 CIMS. It is possible that some of dimeric HOM-ONs are fragmented to $\text{C}_{10}\text{H}_{17}\text{NO}_8$ during nitrate-
265 CIMS measurements. In a recent study by Li et al. (2024), $\text{C}_{10}\text{H}_{17}\text{NO}_8$ was also identified during
266 the synergistic oxidation of α -pinene by O_3 and NO_3 . However, the exact origin of this species
267 remains to be clarified.

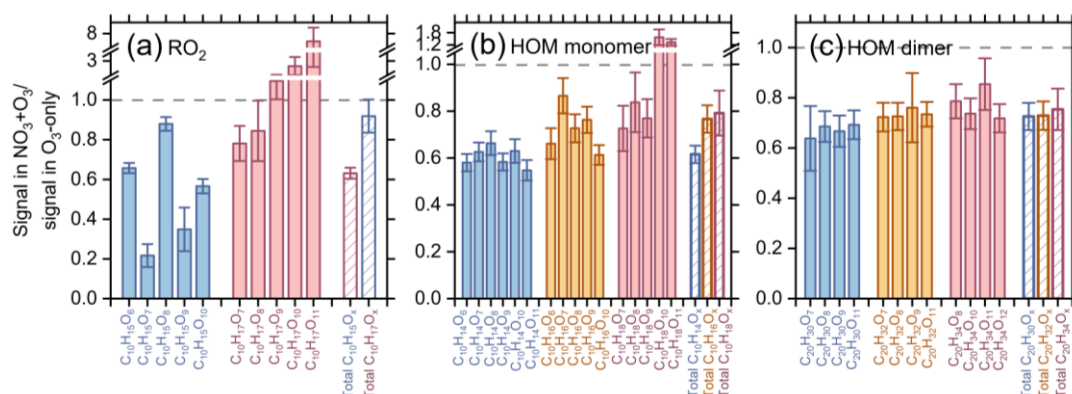
268 The C_{20} dimers with only one nitrogen atom are very likely to be formed from the cross reactions
269 of ClRO_2 or OHRO_2 with NO_3RO_2 , which provides direct evidence for the synergistic RO_2 chemistry
270 in the $\text{O}_3 + \text{NO}_3$ regime. The CHON_2 dimers were also observed in the $\text{O}_3 + \text{NO}_3$ regime, despite
271 their much lower signals than CHON dimers, which is different from the recent studies by Bates et
272 al. (2022) and Li et al. (2024), which found CHON_2 dimer account for an important fraction of the
273 total dimer signals in the synergistic oxidation regime. A potential explanation for this discrepancy
274 is the difference in the instrument sensitivity in these studies (Section 2.1). In general, the nitrate-
275 CIMS has lower sensitivities to ONs than to the $\text{C}_x\text{H}_y\text{O}_z$ -HOM counterparts (Shen et al., 2022;
276 Hyttinen et al., 2015). Bates et al. (2022) used CF_3O^- as the reagent ion of CIMS. Its sensitivity to

277 ONs might be significantly higher than the nitrate ion. In addition, Li et al. (2024) observed a
278 significantly lower signal contribution of CHON₂ dimers using CI-Orbitrap with nitrate reagent ions
279 than with ammonium ions. Despite both using nitrate reagent ions, the nitrate CI-Orbitrap in Li et al.
280 (2024) possibly exhibits higher sensitivities to ONs than the nitrate-CIMS in our study.

281 3.2 Synergistic reaction efficiencies of different RO₂ species

282 In the O₃ + NO₃ regime, synergistic reactions are likely to occur between ^{Cl}RO₂, ^{OH}RO₂ and ^{NO₃}RO₂.
283 Figure 2 shows the Δ[α-pinene]_{O₃}-normalized signal ratios of specific C₁₀ RO₂ as well as their
284 related C_xH_yO_z-HOM monomers and dimers in the synergistic O₃ + NO₃ regime vs. the O₃-only
285 regime. It should be noted that the second-generation oxidation processes are strongly inhibited by
286 the excess of α-pinene in this study, thus the predominant type of RO₂ observed here is primary RO₂.
287 Model simulations show that the H-abstraction of α-pinene by OH radicals contributes less than 2%
288 to the formation of C₁₀H₁₅O_x-RO₂ and related HOMs under different experimental conditions
289 (Figure S5). Therefore, C₁₀H₁₅O_x-RO₂ observed in this study are primarily ^{Cl}RO₂. Notably, the
290 ^{Cl}RO₂ (C₁₀H₁₅O_x) and related C₁₀H₁₄O_x-HOMs decrease by ~30 – 60% in the O₃ + NO₃ regime
291 (Figures 2 a, b), while the decreasing extent of ^{OH}RO₂ (C₁₀H₁₇O_x) and related C₁₀H₁₈O_x-HOMs are
292 significantly smaller (0 – 40%). In particular, some of the most oxygenated C₁₀H₁₇O_x-RO₂ and
293 C₁₀H₁₈O_x-HOMs (x ≥ 9) even increase unexpectedly in the synergistic oxidation regime. For the
294 C₁₀H₁₆O_x-HOMs that can be derived from the self/cross reactions of both ^{Cl}RO₂ and ^{OH}RO₂, their
295 reductions are at a medium level. Because of the very small contribution of acyl RO₂ to the total C₁₀
296 RO₂ (0.4%) (Zang et al., 2023), their consumption by NO₂ leads to less than 2% reduction in the
297 C₁₀ ^{Cl}RO₂ signals. Therefore, the more significant decrease in signals of ^{Cl}RO₂ and related HOMs
298 as compared to the OH-derived ones in the synergistic O₃ + NO₃ regime is primarily due to the more
299 efficient cross reactions of ^{NO₃}RO₂ with ^{Cl}RO₂ than with ^{OH}RO₂. Because a large amount of ^{Cl}RO₂
300 is terminated by ^{NO₃}RO₂, fewer ^{Cl}RO₂ are available to terminate ^{OH}RO₂. As a result, more ^{OH}RO₂
301 can undergo autoxidation to form highly oxygenated C₁₀H₁₇O_x-RO₂ and C₁₀H₁₈O_x-HOMs (x ≥ 9),
302 leading to an increase in signals of these species. Consistently, the signals of C₂₀ HOM dimers
303 decrease by 20 – 40% in the O₃ + NO₃ regime compared to that in O₃-only regime, and the signal
304 reduction of dimers (C₂₀H₃₀O_x) formed by ^{Cl}RO₂ is slightly larger than that of the dimers (C₂₀H₃₄O_x)
305 arising from ^{OH}RO₂ (Figure 2c). Note that the highly oxygenated C₂₀H₃₄O_x dimers (x ≥ 13) that can

306 be formed from self/cross reactions of $C_{10}H_{17}O_x-RO_2$ ($x \geq 9$) are not observed in this study, likely
 307 due to their low abundance and the limitation of instrument sensitivity.



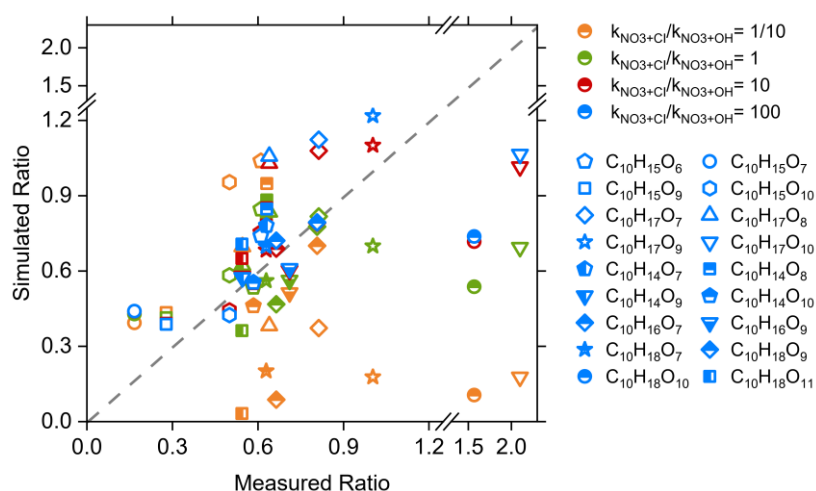
308
 309 Figure 2. Normalized signal ratios of (a) specific and total $C_{10}H_{15,17}O_x-RO_2$ radicals, as well as their
 310 related (b) C_{10} HOM monomers and (c) C_{20} HOM dimers in the $O_3 + NO_3$ regime vs. the O_3 -only
 311 regime (Exps 1-10). Ion signals observed in each oxidation regime are normalized to $\Delta[\alpha\text{-pinene}]_{O_3}$.

312 The above results are somewhat different from the most recent study by Li et al. (2024), which
 313 found that the measured $C_{10}H_{15}O_x-RO_2$ increased slightly with NO_3 radicals while $C_{10}H_{17}O_{5,7}-RO_2$
 314 from OH chemistry decreased by a factor of 9. Li et al. (2024) indicated that additional $C_{10}H_{15}O_x$
 315 could be produced from the H-abstraction pathway of NO_3 oxidation of α -pinene. However, in the
 316 monoterpene oxidation system, the rate constant for H-abstraction by NO_3 radicals is $(4 - 10) \times 10^{-17}$
 317 $cm^3 \text{ molecule}^{-1} \text{ s}^{-1}$, which is $10^3 - 10^4$ times lower than that for the NO_3 addition channel (Martinez
 318 et al., 1998). Besides, the subsequent reactions of RO_2 species formed from H-abstraction by NO_3
 319 radicals should be very similar to those derived from H-abstraction by OH radicals, which was found
 320 not important for $C_xH_yO_z$ -HOM formation in the absence of NO (Zang et al., 2023). Therefore, the
 321 H-abstraction of α -pinene by NO_3 radicals would have negligible influence on $C_{10}H_{15}O_x$ formation.
 322 As Li et al. (2024) used a low α -pinene concentration and relatively high O_3 and NO_3 concentrations
 323 in their experiments, the secondary oxidation of aldehydes, such as the substantially formed
 324 pinonaldehyde, by NO_3 radicals might be important, which could contribute to the additional
 325 formation of $C_{10}H_{15}O_x-RO_2$. However, as noted above, the second-generation oxidation processes
 326 are strongly inhibited due to the excess of α -pinene in this study, therefore the formation of
 327 secondary $C_{10}H_{15}O_x-RO_2$ is not important.

328 In addition, Li et al. (2024) reported that the fraction of α -pinene oxidized by OH radicals decreased
 329 from 44% in the O_3 oxidation system to 6% in the $O_3 + NO_3$ system, mainly due to the depletion of

330 OH radicals by NO_2 and the competitive consumption of α -pinene by NO_3 radicals, which resulted
 331 in a significant decrease in $\text{C}_{10}\text{H}_{17}\text{O}_{5,7}$ radicals from OH chemistry as observed in their experiments.
 332 However, in the present study, because of the excess of α -pinene, over 97% of OH radicals react
 333 with α -pinene and the depletion of OH by NO_2 is minor (0.2 – 1.3%) in the $\text{O}_3 + \text{NO}_3$ regime. The
 334 reduction in the reacted α -pinene by OH radicals is less than 10% compared to the O_3 -only regime.
 335 As a result, a smaller decrease in $\text{C}_{10}\text{H}_{17}\text{O}_{5,7}$ radicals was observed in our study.

336 To gain quantitative constraints on the relative reaction efficiency of $\text{NO}_3\text{RO}_2 + \text{ClRO}_2$ vs. $\text{NO}_3\text{RO}_2 +$
 337 OHRO_2 (i.e., $k_{\text{NO}_3+\text{Cl}}/k_{\text{NO}_3+\text{OH}}$), the signal ratios of $\text{C}_{10}\text{-ClRO}_2$ and OHRO_2 as well as their related C_{10}
 338 HOMs in the synergistic oxidation regime vs. the O_3 -only regime were predicted using a kinetic
 339 model (see Section 2.3) with different $k_{\text{NO}_3+\text{Cl}}/k_{\text{NO}_3+\text{OH}}$ ratios. Figure 3 shows a measurement-model
 340 comparison of those signal ratios. When the ratio of $k_{\text{NO}_3+\text{Cl}}/k_{\text{NO}_3+\text{OH}}$ is smaller than or equal to 1,
 341 the simulated signal ratios of many RO_2 and HOMs differ significantly from the measured ratios,
 342 especially for some $\text{C}_{10}\text{H}_{17}\text{O}_x\text{-RO}_2$ and $\text{C}_{10}\text{H}_{18}\text{O}_x\text{-HOMs}$. When the ratio of $k_{\text{NO}_3+\text{Cl}}/k_{\text{NO}_3+\text{OH}}$ is 10 –
 343 100, there is a good measurement-model agreement for most of RO_2 and HOMs. Therefore, we
 344 conclude that the cross-reaction rate constants of $\text{NO}_3\text{RO}_2 + \text{ClRO}_2$ are on average 10 – 100 times
 345 larger than those for $\text{NO}_3\text{RO}_2 + \text{OHRO}_2$. This different RO_2 cross-reaction efficiency is the main
 346 reason for the significantly larger decrease in the abundance of ClRO_2 and related HOMs as
 347 compared to the OH-derived ones (see Figure 2).

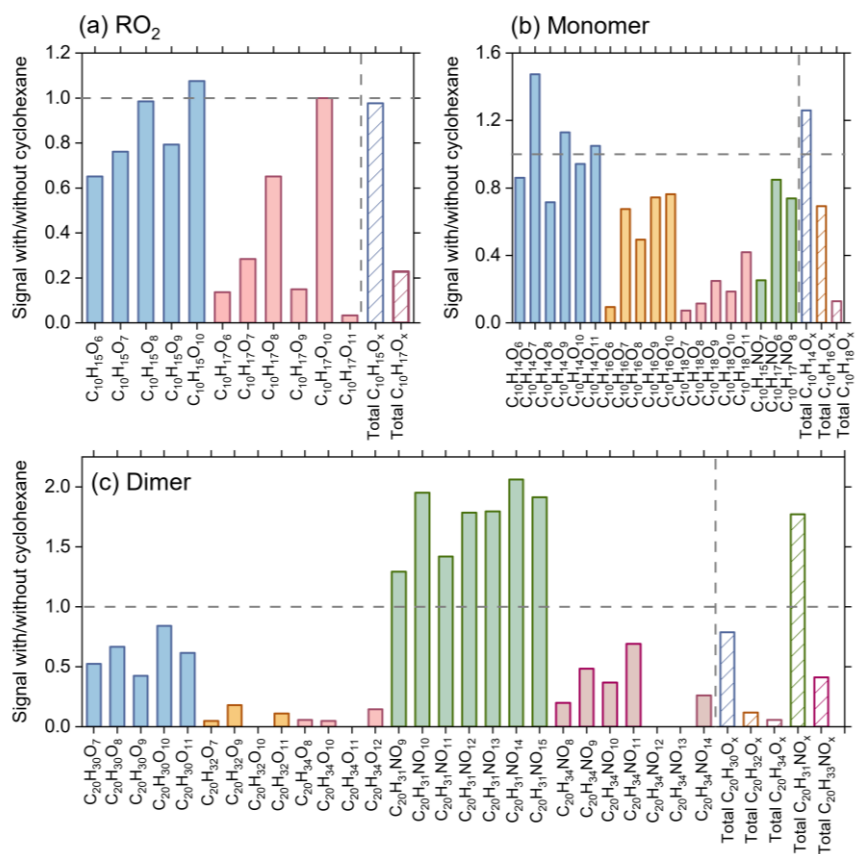


348
 349 Figure 3. Measurement-model comparisons of the signal ratios of different C_{10} RO_2 and HOMs in
 350 the synergistic $\text{O}_3 + \text{NO}_3$ regime vs. the O_3 -only regime. The cross reaction rate constant of NO_3RO_2
 351 + ClRO_2 was set to $2 \times 10^{-12} \text{ cm}^3 \text{ molecule}^{-1} \text{ s}^{-1}$ and the rate of $\text{NO}_3\text{RO}_2 + \text{OHRO}_2$ was varied from $2 \times$
 352 $10^{-11} \text{ cm}^3 \text{ molecule}^{-1} \text{ s}^{-1}$ to $2 \times 10^{-14} \text{ cm}^3 \text{ molecule}^{-1} \text{ s}^{-1}$ in the model.

353 As a competitive reaction pathway, the autoxidation rates of RO₂ can affect the extent to which RO₂
354 cross reactions influence the RO₂ fate and HOM formation. Therefore, sensitivity analyses of the
355 autoxidation rate of RO₂ were conducted to evaluate its influence on the changes of RO₂ and related
356 HOM concentrations in the synergistic O₃ + NO₃ regime vs. the O₃-only regime (Figure S7). In
357 these analyses, a k_{NO₃+Cl}/k_{NO₃+OH} ratio of 10 was used according to the above discussions. As the
358 autoxidation rate of ^{OH}RO₂ increases from 0.28 to 10 s⁻¹, corresponding to the rate range reported in
359 previous studies (Berndt et al., 2016; Zhao et al., 2018; Xu et al., 2019), the simulated reduction of
360 highly oxygenated ^{OH}RO₂ and related C₁₀H₁₈O_x-HOMs in the synergistic O₃ + NO₃ regime exhibits
361 a slight decrease (< 9%) but still agrees reasonably well with the measured value (Figures S7 a-d).
362 Considering that the autoxidation rates of ^{Cl}RO₂ used in the model approach their upper limits
363 reported in the literature, i.e., ~1 s⁻¹ for the butyl ring-opened C₁₀H₁₅O₄-RO₂ (Iyer et al., 2021) and
364 relatively smaller rates for ring-retained C₁₀H₁₅O₄-RO₂ (0.02 – 0.29 s⁻¹, see Scheme S1) (Zhao et
365 al., 2021), we also lowered the autoxidation rate constants of ^{Cl}RO₂ by a factor of 10 to see its
366 influence on RO₂ and HOM distribution in the O₃ + NO₃ regime. The simulated reduction of ^{Cl}RO₂
367 and C₁₀H₁₄O_x-HOMs in this case decreases by 10 – 16% (Figures S7 e-h), while that of C₁₀H₁₆O_x-
368 HOMs increases by up to 30% (Figures S7 i, j). However, the simulated results are still close to the
369 measured values. These sensitivity analyses suggest that the uncertainty in the autoxidation rates of
370 ^{OH}RO₂ and ^{Cl}RO₂ could slightly affect the simulated distribution of RO₂ and HOMs across different
371 oxidation regimes but not significantly change the k_{NO₃+Cl}/k_{NO₃+OH} ratio obtained in this study.
372 Further sensitivity analyses on the rate constant and dimer formation branching ratio of RO₂ cross
373 reactions indicate that the uncertainties in these reaction kinetics do not alter the conclusion
374 regarding the k_{NO₃+Cl}/k_{NO₃+OH} ratio either (see details in Sections S2 and S3).

375 Cyclohexane was added in some experiments as an OH scavenger to elucidate the role of ^{OH}RO₂
376 chemistry in HOM formation in the O₃ + NO₃ regime. In the presence of cyclohexane, ^{OH}RO₂
377 (C₁₀H₁₇O_x) and related HOM monomers (C₁₀H₁₈O_x) and dimers (C₂₀H₃₂O_x and C₂₀H₃₄O_x) decrease
378 by more than 80% (Figure 4), while ^{Cl}RO₂ (C₁₀H₁₅O_x) and related HOM monomers (C₁₀H₁₄O_x) and
379 dimers (C₂₀H₃₀O_x) only decrease slightly (< 30%), in a good agreement with previous measurements
380 (Zhao et al., 2018; Zang et al., 2023). The C₁₀H₁₆O_x species, which can arise from both ^{Cl}RO₂ and
381 ^{OH}RO₂, exhibit a medium reduction (Figure 4b). It is interesting to note that with the addition of

382 cyclohexane, there is a significant increase in $C_{20}H_{31}NO_x$, which are formed from the cross reactions
 383 of $^{\text{Cl}}\text{RO}_2$ with $^{\text{NO}_3}\text{RO}_2$. Such an enhanced production of $C_{20}H_{31}NO_x$ as compared to the slightly
 384 decreased formation of $C_{20}H_{30}O_x$ indicates that the $^{\text{Cl}}\text{RO}_2 + ^{\text{NO}_3}\text{RO}_2$ reactions are competitive
 385 compared to the $^{\text{Cl}}\text{RO}_2 + ^{\text{Cl}}\text{RO}_2$ and $^{\text{Cl}}\text{RO}_2 + ^{\text{OH}}\text{RO}_2$ reactions. As a result, when the $^{\text{OH}}\text{RO}_2$ are
 386 depleted, the $^{\text{Cl}}\text{RO}_2$ that are supposed to react with $^{\text{OH}}\text{RO}_2$, efficiently react with $^{\text{NO}_3}\text{RO}_2$ to form
 387 $C_{20}H_{31}NO_x$, leading to the increase in $C_{20}H_{31}NO_x$ signals. Consistent with the experimental
 388 measurements, the model simulations show that the concentrations of $C_{20}H_{31}NO_x$ in the $\text{O}_3 + \text{NO}_3$
 389 regime increase with the addition of cyclohexane as an OH scavenger (Figure S9). However, the
 390 simulated enhancement is slightly lower than the measurements, which might be due to the
 391 uncertainties in the RO_2 cross-reaction kinetics in the model.

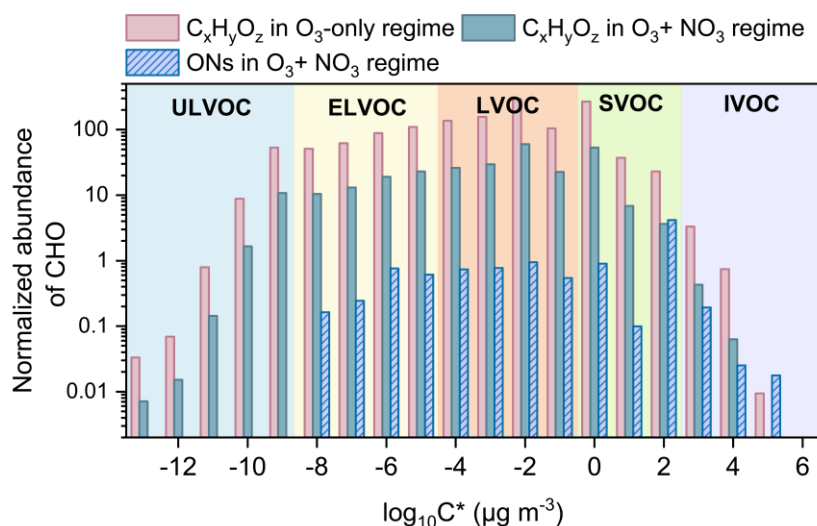


392
 393 Figure 4. Relative changes in signals of (a) C_{10} RO_2 , (b) C_{10} HOMs, and (c) C_{20} dimers due to the
 394 addition of 100 ppm cyclohexane as an OH scavenger derived in the synergistic $\text{O}_3 + \text{NO}_3$ regime
 395 (Exps 7 and 12).

396 3.3 Influence of synergistic oxidation on low-volatility organics and particle formation

397 Compared to the O_3 -only regime, there are a remarkable reduction in $\text{C}_x\text{H}_y\text{O}_z$ -HOMs and a strong

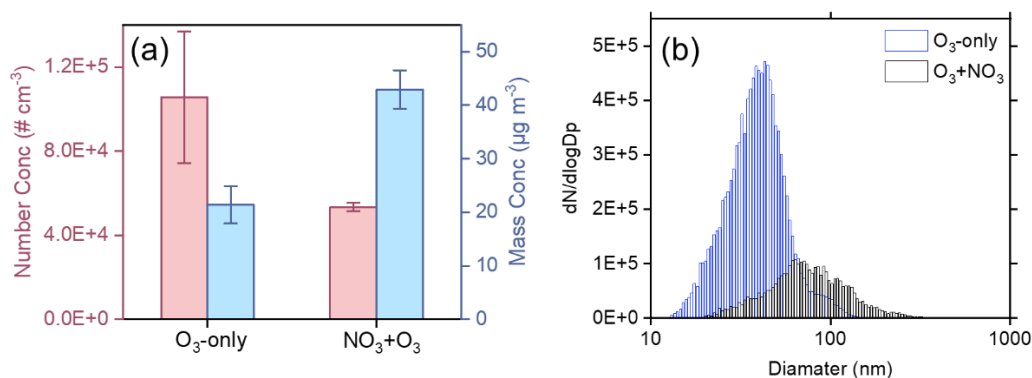
398 formation of HOM-ONs due to the efficient cross reactions between NO_3RO_2 and ClRO_2 in the
 399 synergistic oxidation regime. This significant change in HOM composition and abundance would
 400 alter the volatility distribution of HOMs and influence the formation of particles. The volatilities of
 401 HOMs formed in the two oxidation regimes are estimated using a modified composition-activity
 402 method (see Section 2.2) and shown in Figure 5. The abundance of $\text{C}_x\text{H}_y\text{O}_z$ -HOMs characterized as
 403 ULVOCs and ELVOCs decreases considerably in the synergistic $\text{O}_3 + \text{NO}_3$ regime compared to the
 404 O_3 -only regime (Figure 5a), in agreement with the very recent observations by Li et al. (2024) who
 405 found that the presence of NO_3 radicals during α -pinene ozonolysis significantly reduced the
 406 abundance of ULVOCs. Although substantial amounts of HOM-ONs are formed in the $\text{O}_3 + \text{NO}_3$
 407 regime, they generally have higher volatilities (i.e., characterized as ELVOCs to IVOCs) (Figure
 408 5b). Therefore, the synergistic $\text{O}_3 + \text{NO}_3$ oxidation of α -pinene significantly reduces the formation
 409 of ULVOCs and increases the overall volatility of total HOMs.



410
 411 Figure 5. Volatility distribution of $\text{C}_x\text{H}_y\text{O}_z$ -HOMs and HOM-ONs formed in the $\text{O}_3 + \text{NO}_3$ regime
 412 and O_3 -only regime (Exps 1, 6). Ion signals in each oxidation regime are normalized to the
 413 corresponding total reacted α -pinene.

414 Figure 6a shows the particle number and mass concentrations formed in the two oxidation regimes
 415 in SOA formation experiments (Table S1, Exps 13, 14). The particle number concentration decreases
 416 by more than 50% whereas the particle mass concentration increases by a factor of 2 in the
 417 synergistic $\text{O}_3 + \text{NO}_3$ regime, compared to that in the O_3 -only regime. The presence of NO_3 radicals
 418 during α -pinene ozonolysis reduces the abundance of ULVOCs, which are the key species driving
 419 particle nucleation, thereby leading to a reduction in the particle number concentration in the $\text{O}_3 +$

420 NO₃ regime. On the other hand, substantial formation of HOM-ONs is expected from the cross
 421 reactions of ^fNO₃RO₂ with ^CIRO₂ and ^{OH}RO₂ in the synergistic oxidation regime (Li et al., 2024; Bates
 422 et al., 2022), although their signals are relatively low due to the low sensitivity of nitrate-CIMS to
 423 ONs in this study. The newly formed HOM-ONs have relatively higher volatilities and are
 424 inefficient in initiating particle nucleation, but they are able to partition into the formed particles
 425 and contribute to the particle mass growth. Meanwhile, as the particle number concentration
 426 decreases drastically in the synergistic oxidation regime, more condensable vapors are available for
 427 each particle to grow to larger sizes (Figure 6b), which would in turn favor the condensation of more
 428 volatile organic species including ONs due to the reduced curvature effect of the larger particles,
 429 ultimately resulting in an increase in SOA mass concentrations.



430

431 Figure 6. Number and mass concentrations (a), as well as the size distribution (b) of particles formed
 432 from the ozonolysis and synergistic O₃ + NO₃ oxidation of α -pinene (Exps 13-14).

433 Recently, Bates et al. (2022) also found that in chamber experiments with seed particles, the SOA
 434 mass yields were significantly higher during α -pinene oxidation by O₃ + NO₃ than during ozonolysis,
 435 mainly due to the substantial formation and condensation of ON dimers. However, in the absence
 436 of seed particles, synergistic O₃ + NO₃ oxidation of α -pinene does not nucleate in their study. This
 437 phenomenon might be due to the high concentrations of NO₂ (72 ppb) and O₃ (102 ppb) as well as
 438 the relatively low concentration of α -pinene (27 ppb) in their experiments. As indicated by Bates et
 439 al. (2022), under this conditions NO₃ radicals were substantially formed and contributed to a
 440 dominant fraction (75%) of α -pinene oxidation, which strongly inhibited the production of low-
 441 volatility species and particle nucleation.

442 3.4 Atmospheric relevance of experimental results

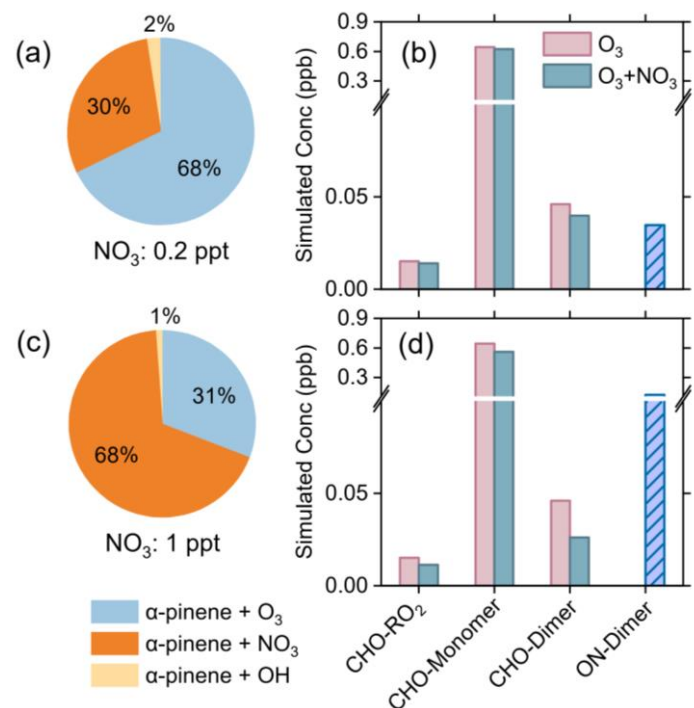
443 In the present study, the flow tube experiments were conducted under dry conditions. Although
444 water vapor may affect the fate of Criegee intermediates (CIs) and RO₂ radicals and thereby HOM
445 formation during the oxidation of organics under humid conditions, there is growing evidence that
446 such effects in the α -pinene oxidation system are small. Kinetics studies have found that the
447 stabilized Criegee intermediates (SCIs) arising from α -pinene ozonolysis can undergo fast
448 unimolecular decay at a rate constant of 60 – 250 s⁻¹ (Vereecken et al., 2017; Newland et al., 2018),
449 which is rapid compared to their reaction with water vapor, in particular for syn-SCIs, under
450 atmospheric conditions (Vereecken et al., 2017; Newland et al., 2018). In addition, the yield of OH
451 radicals from CI decomposition is independent of RH (Atkinson et al., 1992; Aschmann et al., 2002).
452 Consistent with the fast unimolecular reaction kinetics revealed by these studies, recent laboratory
453 measurements have shown that the contribution of SCIs to the formation of gas-phase and particle-
454 phase dimers are small (<20%) during α -pinene ozonolysis (Zhao et al., 2018; Zhao et al., 2022).
455 Furthermore, the molecular composition and abundance of HOM monomers and dimers (Li et al.,
456 2019) and the formation of particle-phase dimers (Zhang et al., 2015; Kenseth et al., 2018) do not
457 change significantly with RH ranging from 3% to 92%. These studies suggest that the humidity
458 condition does not strongly affect the HOM formation chemistry in the α -pinene ozonolysis system.

459 To evaluate the relevance of our experimental findings to the real atmosphere, we performed
460 chemical model simulations of HOM formation from nocturnal synergistic O₃ + NO₃ oxidation of
461 α -pinene under typical atmospheric conditions. In these simulations, constant concentrations of α -
462 pinene (1 ppb), O₃ (30 ppb), NO (5 ppt), NO₂ (1.8 ppb), NO₃ radicals (0.2 or 1 ppt), OH radicals (5
463 – 50 × 10⁴ molecules cm⁻³), HO₂ radicals (4 ppt), as well as a constant RH of 50% and temperature
464 of 298 K were used as typical nocturnal conditions in the boreal forest according to the field studies
465 (Stone et al., 2012; Lee et al., 2016a; Brown and Stutz, 2012; Geyer et al., 2003b; Kristensen et al.,
466 2016; Hakola et al., 2012; Liebmann et al., 2018). Considering the rapid deposition of oxidized
467 biogenic compounds (Nguyen et al., 2015), a typical dilution lifetime of 5 h (i.e., $k_{\text{dil}} = 1/5 \text{ h}^{-1}$) was
468 assumed in the model. According to the above analysis, the cross-reaction rate constants for ^{NO₃}RO₂
469 + ^{CI}RO₂ and ^{NO₃}RO₂ + ^{OH}RO₂ were set to 1 × 10⁻¹² cm³ molecule⁻¹ s⁻¹ and 1 × 10⁻¹³ cm³ molecule⁻¹
470 s⁻¹ in the model, respectively. The formation of RO₂ with oxygen numbers higher than 11 was not

471 considered in the model, due to the large uncertainty in the autoxidation rate constants of the highly
472 oxygenated RO₂. In fact, the autoxidation rate of the highly oxygenated RO₂ is expected to be small
473 given the significant decrease in the number of active sites for intramolecular H-abstraction in the
474 molecule. As a result, the contribution of the most oxygenated HOMs to the total HOM monomers
475 could be relatively small (Zhao et al., 2018; Clafin et al., 2018).

476 In the absence of NO₃ radicals (with NO₃ concentrations and formation rates set to zero), the amount
477 of α -pinene consumed during 4 hours of simulation is 1.04 ppb. When a relatively low NO₃
478 concentration (0.2 ppt) is considered (Figure 7a), the amount of α -pinene consumed is 1.48 ppb, and
479 the ozonolysis is the primary loss pathway of α -pinene (68%), followed by NO₃ (30%) and OH
480 oxidation (2%). The reactions of RO₂ + HO₂, RO₂ + NO, and RO₂ + RO₂ account for ~49%, ~27%,
481 and ~24% of the total RO₂ fate, respectively (Figure S10a). Compared to the ozonolysis of α -pinene,
482 the synergistic O₃ + NO₃ oxidation leads to a reduction of 3% and 13% in the formation of C_xH_yO_z-
483 HOM monomers and dimers, respectively (Figure 7b). Given that the concentrations of α -pinene
484 and oxidants were held constant during the simulation, the consumptions of α -pinene by O₃ and OH
485 radicals are the same across different oxidation regimes. Therefore, the decreases in the
486 concentrations of C_xH_yO_z-HOM monomers and dimers in the presence of NO₃ oxidation are mainly
487 due to the cross reactions of ^{NO₃}RO₂ with other RO₂. When the NO₃ concentration is as high as 1
488 ppt as reported in field studies (Liebmann et al., 2018), the consumption of α -pinene reaches 3.24
489 ppb, of which 68% is contributed by NO₃ oxidation (Figure 7c). Under this condition, the RO₂ +
490 RO₂ reactions account for ~34% of the total RO₂ fate (Figure S10b). As a result, the cross reactions
491 of ^{NO₃}RO₂ with other RO₂ play a more important role in the HOM formation. The production of
492 C_xH_yO_z-HOM monomers and dimers decreases by 13% and 43%, respectively, due to the presence
493 of NO₃ oxidation (Figure 7d). We note that the variation in RH from 0-90% in the model has negligible
494 influence on the relative changes in C_xH_yO_z-HOMs under these nocturnal atmospheric conditions (Figure
495 S11). Considering that there are uncertainties in the dilution rate constant, a sensitivity analysis was
496 performed by varying the k_{dil} in the range of 0.04 – 0.2 h⁻¹. It is found that the variation within these
497 rate values does not significantly influence the response of C_xH_yO_z-HOM dimer formation to
498 concurrent NO₃ oxidation (Figure S12).

499



500

501 Figure 7. Model simulations of α -pinene oxidation and HOM formation under typical nighttime
 502 conditions in the boreal forest. (a, c) Contributions of different loss pathways of α -pinene by
 503 different oxidants at NO_3 concentrations of 0.2 and 1 ppt, respectively; (b, d) Concentrations of
 504 $\text{C}_x\text{H}_y\text{O}_z$ -HOMs and HOM-ONs formed by synergistic $\text{O}_3 + \text{NO}_3$ oxidation and ozonolysis of α -
 505 pinene under conditions corresponding to (a) and (c). The simulations were run for 4 h after an 8-h
 506 spin-up for intermediates and secondary species.

507 Field observations have shown that NO_3 radicals, O_3 , and OH radicals all had important
 508 contributions to monoterpene oxidation during the early morning after sunrise and late afternoon
 509 before sunset in the southeastern United States (Zhang et al., 2018). In addition, relatively high
 510 nighttime OH concentrations of $(2 - 10) \times 10^5$ molecules cm^{-3} were measured in some areas such
 511 as Germany and New York City (Faloona et al., 2001; Geyer et al., 2003a). As a result, a model
 512 simulation was conducted using a 10 times higher OH concentration (5×10^5 molecules cm^{-3}). The
 513 concentration of NO_3 radicals is 1 ppt and the concentrations of other species are the same as the
 514 values mentioned above. With a higher OH concentration, O_3 , NO_3 , and OH radicals account for
 515 28%, 62%, and 10% to the total α -pinene consumption, respectively (Figure S13 a). Compared to
 516 the results under low OH concentration, the formation of $\text{C}_x\text{H}_y\text{O}_z$ -HOM monomers and dimers are
 517 all enhanced under high OH concentration (Figure S13 b). This is mainly due to the promoted
 518 self/cross reactions of $^{\text{OH}}\text{RO}_2$, as well as the promoted formation of $\text{C}_{10}\text{H}_{15}\text{O}_x\text{-RO}_2$ derived from H-
 519 abstraction pathway by OH radicals. Nevertheless, the presence of NO_3 oxidation still reduces the

520 formation of $C_xH_yO_z$ -HOM dimers by 26% (Figure S13 b).

521 Furthermore, model simulations for conditions typical of the southeastern United States (see details
522 in Section S4) suggest that the coexistence of isoprene appears to exacerbate the suppression effect
523 of synergistic oxidation on HOM formation from monoterpenes. As shown in Figure S14, in the
524 absence of isoprene, the synergistic $O_3 + NO_3$ oxidation of α -pinene leads to a reduction of 13% and
525 24% in the formation of $C_xH_yO_z$ -HOM monomers and dimers, respectively. When isoprene is
526 present, as the isoprene + NO_3 oxidation produces a significant amount of nitrooxy RO_2 that can
527 also scavenge α -pinene-derived $^{Cl}RO_2$ and $^{OH}RO_2$ via cross reactions, the synergistic oxidation leads
528 to a slightly larger reduction in $C_xH_yO_z$ -HOM monomers and dimers (15% and 31%, respectively).

529 The above model simulations suggest that under nocturnal atmospheric conditions with a very low
530 NO_3 concentration, the RO_2 radical pool is dominated by $^{Cl}RO_2$ and their self/cross reactions are a
531 major contributor to ULVOCs such as the highly oxygenated C_{20} dimers as observed in boreal forest
532 (Bianchi et al., 2017). When the NO_3 concentration is high, the production of $^{NO_3}RO_2$ becomes
533 significant and their cross reactions with $^{Cl}RO_2$ would suppress the formation of ULVOCs. Although
534 HOM-ON dimers are readily produced by cross reactions between $^{NO_3}RO_2$ and $^{Cl}RO_2$, they generally
535 have higher volatilities than $C_xH_yO_z$ -HOM dimers and therefore are less efficient in initiating
536 particle formation. However, these HOM-ONs can be an important contributor to the particle mass
537 growth. As suggested by the model simulations in Bates et al. (2022), the NO_3 oxidation of α -pinene
538 led to a particulate nitrate yield of 7% under nocturnal atmospheric conditions in rural Alabama
539 during the SOAS campaign. Our results offer mechanistic and quantitative insights on how the
540 synergistic oxidation of α -pinene by O_3 and NO_3 radicals can influence the formation of low-
541 volatility organic compounds and hence particle formation and growth. They also provide a potential
542 explanation for field observations that NPF events frequently occur in monoterpene-rich regions
543 during daytime but not at nighttime (Mohr et al., 2017; Kulmala et al., 2001; Junninen et al., 2017).

544 **4. Conclusions**

545 This study provides a comprehensive characterization of the nocturnal synergistic oxidation of α -
546 pinene by O_3 and NO_3 radicals and its influence on the formation of HOMs and low-volatility
547 organic compounds using a combination of flow reactor experiments and detailed kinetic model
548 simulations. It is found that the formation of $C_xH_yO_z$ -HOMs in the $O_3 + NO_3$ regime is significantly

549 suppressed compared to that in the O₃-only regime, mainly due to the depletion of ozonolysis-
550 derived RO₂ (i.e., ^{Cl}RO₂ and ^{OH}RO₂) by ^{NO₃}RO₂ via cross reactions. In addition, the decreases in the
551 abundance of ^{Cl}RO₂ and related HOMs are significantly larger than those of OH-derived ones,
552 indicating that the ^{NO₃}RO₂ species react more efficiently with ^{Cl}RO₂ than with ^{OH}RO₂. Detailed
553 measurement-model comparisons for the distribution of a suite of ^{Cl}RO₂, ^{OH}RO₂, and associated
554 HOMs across different oxidation regimes further reveal that the cross reactions between ^{Cl}RO₂ and
555 ^{NO₃}RO₂ are averagely 10 – 100 times more efficient than those of ^{OH}RO₂ and ^{NO₃}RO₂.

556 The suppressed formation of C_xH_yO_z-HOMs in the synergistic O₃ + NO₃ regime results in a
557 significant reduction in ULVOCs. Although substantial amounts of HOM-ONs are formed from the
558 cross reactions between ^{NO₃}RO₂ and ^{Cl}RO₂ or ^{OH}RO₂ in the synergistic oxidation regime, they have
559 higher volatilities and are less likely to participate in the formation and initial growth of new
560 particles. As a result, in our experiment the formation of new particles in the synergistic oxidation
561 regime is substantially inhibited compared to the O₃-only regime. Chemical model simulations
562 further confirm that the synergistic oxidation of α-pinene by O₃ and NO₃ radicals can significantly
563 inhibit the formation of C_xH_yO_z-HOMs, especially the ultra-low volatility C_xH_yO_z-HOM dimers
564 under typical nighttime atmospheric conditions. Our study sheds lights on the synergistic oxidation
565 mechanism of biogenic emissions and underscores the importance of considering this chemistry for
566 a better depiction of the formation of low-volatility organics and particles in the atmosphere.

567

568 *Data availability.* The data presented in this work are available upon request from the corresponding
569 author.

570

571 *Author contributions.* YZ and HZ designed the study, HZ and DH performed the experiments. YZ
572 and HZ analyzed the data, conducted model simulations, and wrote the paper. All other authors
573 contributed to discussion and writing.

574 *Competing interests.* The authors declare no conflict of interest.

575

576 *Acknowledgments.* This work was supported by the National Natural Science Foundation
577 of China (grants 22376137 and 22022607). Dan Dan Huang acknowledges the financial
578 support from the Science and Technology Commission of Shanghai Municipality (grant
579 21230711000).

580 **References**

- 581 Aschmann, S. M., Arey, J., and Atkinson, R.: OH radical formation from the gas-phase reactions of O₃
582 with a series of terpenes, *Atmos. Environ.*, 36, 4347-4355, [https://doi.org/10.1016/S1352-](https://doi.org/10.1016/S1352-2310(02)00355-2)
583 2310(02)00355-2, 2002.
- 584 Atkinson, R., Aschmann, S. M., Arey, J., and Shorees, B.: Formation of OH radicals in the gas-phase
585 reactions of O₃ with a series of terpenes, *J. Geophys. Res.-Atmos.*, 97, 6065-6073,
586 <https://doi.org/10.1029/92JD00062>, 1992.
- 587 Ayres, B. R., Allen, H. M., Draper, D. C., Brown, S. S., Wild, R. J., Jimenez, J. L., Day, D. A.,
588 Campuzano-Jost, P., Hu, W., de Gouw, J., Koss, A., Cohen, R. C., Duffey, K. C., Romer, P.,
589 Baumann, K., Edgerton, E., Takahama, S., Thornton, J. A., Lee, B. H., Lopez-Hilfiker, F. D., Mohr,
590 C., Wennberg, P. O., Nguyen, T. B., Teng, A., Goldstein, A. H., Olson, K., and Fry, J. L.: Organic
591 nitrate aerosol formation via NO₃ + biogenic volatile organic compounds in the southeastern United
592 States, *Atmos. Chem. Phys.*, 15, 13377-13392, <https://doi.org/10.5194/acp-15-13377-2015>, 2015.
- 593 Bates, K. H., Burke, G. J. P., Cope, J. D., and Nguyen, T. B.: Secondary organic aerosol and organic
594 nitrogen yields from the nitrate radical (NO₃) oxidation of alpha-pinene from various RO₂ fates,
595 *Atmos. Chem. Phys.*, 22, 1467-1482, <https://doi.org/10.5194/acp-22-1467-2022>, 2022.
- 596 Berndt, T.: Peroxy radical processes and product formation in the OH radical-initiated oxidation of alpha-
597 pinene for near-atmospheric conditions, *J. Phys. Chem. A*, 125, 9151-9160,
598 <https://doi.org/10.1021/acs.jpca.1c05576>, 2021.
- 599 Berndt, T., Mentler, B., Scholz, W., Fischer, L., Herrmann, H., Kulmala, M., and Hansel, A.: Accretion
600 product formation from ozonolysis and OH radical reaction of alpha-pinene: mechanistic insight
601 and the influence of isoprene and ethylene, *Environ. Sci. Technol.*, 52, 11069-11077,
602 <https://doi.org/10.1021/acs.est.8b02210>, 2018a.
- 603 Berndt, T., Scholz, W., Mentler, B., Fischer, L., Herrmann, H., Kulmala, M., and Hansel, A.: Accretion
604 product formation from self- and cross-reactions of RO₂ radicals in the atmosphere, *Angew. Chem.*
605 *Int. Edit.*, 57, 3820-3824, <https://doi.org/10.1002/anie.201710989>, 2018b.
- 606 Berndt, T., Richters, S., Jokinen, T., Hyttinen, N., Kurtén, T., Otkjær, R. V., Kjaergaard, H. G., Stratmann,
607 F., Herrmann, H., Sipilä, M., Kulmala, M., and Ehn, M.: Hydroxyl radical-induced formation of
608 highly oxidized organic compounds, *Nat. Commun.*, 7, <https://doi.org/10.1038/ncomms13677>,
609 2016.
- 610 Bianchi, F., Garmash, O., He, X. C., Yan, C., Iyer, S., Rosendahl, I., Xu, Z. N., Rissanen, M. P., Riva, M.,
611 Taipale, R., Sarnela, N., Petäjä, T., Worsnop, D. R., Kulmala, M., Ehn, M., and Junninen, H.: The
612 role of highly oxygenated molecules (HOMs) in determining the composition of ambient ions in the
613 boreal forest, *Atmos. Chem. Phys.*, 17, 13819-13831, <https://doi.org/10.5194/acp-17-13819-2017>,
614 2017.
- 615 Bianchi, F., Kurtén, T., Riva, M., Mohr, C., Rissanen, M. P., Roldin, P., Berndt, T., Crouse, J. D.,
616 Wennberg, P. O., Mentel, T. F., Wildt, J., Junninen, H., Jokinen, T., Kulmala, M., Worsnop, D. R.,
617 Thornton, J. A., Donahue, N., Kjaergaard, H. G., and Ehn, M.: Highly oxygenated organic molecules
618 (HOM) from gas-phase autoxidation involving peroxy radicals: a key contributor to atmospheric
619 aerosol, *Chem. Rev.*, 119, 3472-3509, <https://doi.org/10.1021/acs.chemrev.8b00395>, 2019.
- 620 Boyd, C. M., Sanchez, J., Xu, L., Eugene, A. J., Nah, T., Tuet, W. Y., Guzman, M. I., and Ng, N. L.:
621 Secondary organic aerosol formation from the β-pinene+NO₃ system: effect of humidity and peroxy
622 radical fate, *Atmos. Chem. Phys.*, 15, 7497-7522, <https://doi.org/10.5194/acp-15-7497-2015>, 2015.

623 Brown, S. S. and Stutz, J.: Nighttime radical observations and chemistry, *Chem. Soc. Rev.*, 41,
624 <https://doi.org/10.1039/c2cs35181a>, 2012.

625 Claffin, M. S., Krechmer, J. E., Hu, W., Jimenez, J. L., and Ziemann, P. J.: Functional group composition
626 of secondary organic aerosol formed from ozonolysis of α -pinene under high VOC and autoxidation
627 conditions, *ACS Earth Space Chem.*, 2, 1196-1210,
628 <https://doi.org/10.1021/acsearthspacechem.8b00117>, 2018.

629 Daumit, K. E., Kessler, S. H., and Kroll, J. H.: Average chemical properties and potential formation
630 pathways of highly oxidized organic aerosol, *Faraday Discuss.*, 165,
631 <https://doi.org/10.1039/c3fd00045a>, 2013.

632 Donahue, N. M., Epstein, S. A., Pandis, S. N., and Robinson, A. L.: A two-dimensional volatility basis
633 set: 1. organic-aerosol mixing thermodynamics, *Atmos. Chem. Phys.*, 11, 3303-3318,
634 <https://doi.org/10.5194/acp-11-3303-2011>, 2011.

635 Donahue, N. M., Henry, K. M., Mentel, T. F., Kiendler-Scharr, A., Spindler, C., Bohn, B., Brauers, T.,
636 Dorn, H. P., Fuchs, H., Tillmann, R., Wahner, A., Saathoff, H., Naumann, K.-H., Möhler, O., Leisner,
637 T., Müller, L., Reinnig, M.-C., Hoffmann, T., Salo, K., Hallquist, M., Frosch, M., Bilde, M.,
638 Tritscher, T., Barnet, P., Praplan, A. P., DeCarlo, P. F., Dommen, J., Prévôt, A. S. H., and
639 Baltensperger, U.: Aging of biogenic secondary organic aerosol via gas-phase OH radical reactions,
640 *P. Natl. Acad. Sci. USA*, 109, 13503-13508, <https://doi.org/10.1073/pnas.1115186109>, 2012.

641 Ehn, M., Thornton, J. A., Kleist, E., Sipilä, M., Junninen, H., Pullinen, I., Springer, M., Rubach, F.,
642 Tillmann, R., and Lee, B.: A large source of low-volatility secondary organic aerosol, *Nature*, 506,
643 476-479, <https://doi.org/10.1038/nature13032>, 2014.

644 Faloon, I., Tan, D., Brune, W., Hurst, J., Barket, D., Couch, T. L., Shepson, P., Apel, E., Riemer, D.,
645 Thornberry, T., Carroll, M. A., Sillman, S., Keeler, G. J., Sagady, J., Hooper, D., and Paterson, K.:
646 Nighttime observations of anomalously high levels of hydroxyl radicals above a deciduous forest
647 canopy, *J. Geophys. Res.-Atmos.*, 106, 24315-24333, <https://doi.org/10.1029/2000JD900691>, 2001.

648 Fry, J. L., Draper, D. C., Barsanti, K. C., Smith, J. N., Ortega, J., Winkler, P. M., Lawler, M. J., Brown,
649 S. S., Edwards, P. M., Cohen, R. C., and Lee, L.: Secondary organic aerosol formation and organic
650 nitrate yield from NO₃ oxidation of biogenic hydrocarbons, *Environ. Sci. Technol.*, 48, 11944-11953,
651 <https://doi.org/10.1021/es502204x>, 2014.

652 Geyer, A., Bächmann, K., Hofzumahaus, A., Holland, F., Konrad, S., Klüpfel, T., Pätz, H. W., Perner, D.,
653 Mihelcic, D., Schäfer, H. J., Volz-Thomas, A., and Platt, U.: Nighttime formation of peroxy and
654 hydroxyl radicals during the BERLIOZ campaign: Observations and modeling studies, *J. Geophys.*
655 *Res.-Atmos.*, 108, <https://doi.org/10.1029/2001JD000656>, 2003a.

656 Geyer, A., Bächmann, K., Hofzumahaus, A., Holland, F., Konrad, S., Klüpfel, T., Pätz, H. W., Perner, D.,
657 Mihelcic, D., Schäfer, H. J., Volz-Thomas, A., and Platt, U.: Nighttime formation of peroxy and
658 hydroxyl radicals during the BERLIOZ campaign: Observations and modeling studies, *J. Geophys.*
659 *Res.-Atmos.*, 108, <https://doi.org/10.1029/2001JD000656>, 2003b.

660 Hakola, H., Hellén, H., Hemmilä, M., Rinne, J., and Kulmala, M.: In situ measurements of volatile
661 organic compounds in a boreal forest, *Atmos. Chem. Phys.*, 12, 11665-11678,
662 <https://doi.org/10.5194/acp-12-11665-2012>, 2012.

663 Hallquist, M., Wängberg, I., Ljungström, E., Barnes, I., and Becker, K. H.: Aerosol and product yields
664 from NO₃ radical-initiated oxidation of selected monoterpenes, *Environ. Sci. Technol.*, 33, 553-559,
665 <https://doi.org/10.1021/es980292s>, 1999.

666 Huang, R. J., Zhang, Y., Bozzetti, C., Ho, K. F., Cao, J. J., Han, Y., Daellenbach, K. R., Slowik, J. G.,

667 Platt, S. M., Canonaco, F., Zotter, P., Wolf, R., Pieber, S. M., Brun, E. A., Crippa, M., Ciarelli, G.,
668 Piazzalunga, A., Schwikowski, M., Abbaszade, G., Schnelle-Kreis, J., Zimmermann, R., An, Z.,
669 Szidat, S., Baltensperger, U., El Haddad, I., and Prevot, A. S.: High secondary aerosol contribution
670 to particulate pollution during haze events in China, *Nature*, 514, 218-222, 10.1038/nature13774,
671 2014.

672 Huang, W., Saathoff, H., Shen, X., Ramisetty, R., Leisner, T., and Mohr, C.: Chemical characterization
673 of highly functionalized organonitrates contributing to night-time organic aerosol mass loadings and
674 particle growth, *Environ. Sci. Technol.*, 53, 1165-1174, <https://doi.org/10.1021/acs.est.8b05826>,
675 2019.

676 Hyttinen, N., Kupiainen-Määttä, O., Rissanen, M. P., Muuronen, M., Ehn, M., and Kurtén, T.: Modeling
677 the charging of highly oxidized cyclohexene ozonolysis products using nitrate-based chemical
678 ionization, *J. Phys. Chem. A*, 119, 6339-6345, <https://doi.org/10.1021/acs.jpca.5b01818>, 2015.

679 Inomata, S.: New particle formation promoted by OH reactions during α -pinene ozonolysis, *ACS Earth
680 Space Chem.*, 5, 1929-1933, <https://doi.org/10.1021/acsearthspacechem.1c00142>, 2021.

681 Isaacman-VanWertz, G. and Aumont, B.: Impact of organic molecular structure on the estimation of
682 atmospherically relevant physicochemical parameters, *Atmos. Chem. Phys.*, 21, 6541-6563,
683 <https://doi.org/10.5194/acp-21-6541-2021>, 2021.

684 Iyer, S., Rissanen, M. P., Valiev, R., Barua, S., Krechmer, J. E., Thornton, J., Ehn, M., and Kurten, T.:
685 Molecular mechanism for rapid autoxidation in alpha-pinene ozonolysis, *Nat. Commun.*, 12, 878,
686 <https://doi.org/10.1038/s41467-021-21172-w>, 2021.

687 Jenkin, M., Young, J., and Rickard, A.: The MCM v3.3.1 degradation scheme for isoprene, *Atmos. Chem.
688 Phys.*, 15, 11433-11459, <https://doi.org/10.5194/acp-15-11433-2015>, 2015.

689 Jokinen, T., Sipilä, M., Richters, S., Kerminen, V. M., Paasonen, P., Stratmann, F., Worsnop, D., Kulmala,
690 M., Ehn, M., and Herrmann, H.: Rapid autoxidation forms highly oxidized RO₂ radicals in the
691 atmosphere, *Angew. Chem. Int. Edit.*, 53, 14596-14600, <https://doi.org/10.1002/anie.201408566>,
692 2014.

693 Junninen, H., Ehn, M., Petäjä, T., Luosujärvi, L., Kotiaho, T., Kostiainen, R., Rohner, U., Gonin, M.,
694 Fuhrer, K., and Kulmala, M.: A high-resolution mass spectrometer to measure atmospheric ion
695 composition, *Atmos. Meas. Tech.*, 3, 1039-1053, <https://doi.org/10.5194/amt-3-1039-2010>, 2010.

696 Junninen, H., Hulkkonen, M., Riipinen, I., Nieminen, T., Hirsikko, A., Suni, T., Boy, M., Lee, S.-H., Vana,
697 M., Tammet, H., Kerminen, V.-M., and Kulmala, M.: Observations on nocturnal growth of
698 atmospheric clusters, *Tellus B: Chemical and Physical Meteorology*, 60, 365-371,
699 <https://doi.org/10.1111/j.1600-0889.2008.00356.x>, 2017.

700 Kenseth, C. M., Huang, Y., Zhao, R., Dalleska, N. F., Hethcox, J. C., Stoltz, B. M., and Seinfeld, J. H.:
701 Synergistic O₃ + OH oxidation pathway to extremely low-volatility dimers revealed in beta-pinene
702 secondary organic aerosol, *P. Natl. Acad. Sci. USA*, 115, 8301-8306,
703 <https://doi.org/10.1073/pnas.1804671115>, 2018.

704 Kirkby, J., Duplissy, J., Sengupta, K., Frege, C., Gordon, H., Williamson, C., Heinritzi, M., Simon, M.,
705 Yan, C., Almeida, J., Tröstl, J., Nieminen, T., Ortega, I. K., Wagner, R., Adamov, A., Amorim, A.,
706 Bernhammer, A.-K., Bianchi, F., Breitenlechner, M., Brilke, S., Chen, X., Craven, J., Dias, A.,
707 Ehrhart, S., Flagan, R. C., Franchin, A., Fuchs, C., Guida, R., Hakala, J., Hoyle, C. R., Jokinen, T.,
708 Junninen, H., Kangasluoma, J., Kim, J., Krapf, M., Kürten, A., Laaksonen, A., Lehtipalo, K.,
709 Makhmutov, V., Mathot, S., Molteni, U., Onnela, A., Peräkylä, O., Piel, F., Petäjä, T., Praplan, A. P.,
710 Pringle, K., Rap, A., Richards, N. A. D., Riipinen, I., Rissanen, M. P., Rondo, L., Sarnela, N.,

711 Schobesberger, S., Scott, C. E., Seinfeld, J. H., Sipilä, M., Steiner, G., Stozhkov, Y., Stratmann, F.,
712 Tomé, A., Virtanen, A., Vogel, A. L., Wagner, A. C., Wagner, P. E., Weingartner, E., Wimmer, D.,
713 Winkler, P. M., Ye, P., Zhang, X., Hansel, A., Dommen, J., Donahue, N. M., Worsnop, D. R.,
714 Baltensperger, U., Kulmala, M., Carslaw, K. S., and Curtius, J.: Ion-induced nucleation of pure
715 biogenic particles, *Nature*, 533, 521-526, <https://doi.org/10.1038/nature17953>, 2016.

716 Kristensen, K., Watne, Å. K., Hammes, J., Lutz, A., Petäjä, T., Hallquist, M., Bilde, M., and Glasius, M.:
717 High-molecular weight dimer esters are major products in aerosols from α -pinene ozonolysis and
718 the boreal forest, *Environ. Sci. Tech. Lett.*, 3, 280-285, <https://doi.org/10.1021/acs.estlett.6b00152>,
719 2016.

720 Kulmala, M., Hämeri, K., Aalto, P. P., Mäkelä, J. M., Pirjola, L., Nilsson, E. D., Buzorius, G., Rannik,
721 Ü., Dal Maso, M., Seidl, W., Hoffman, T., Janson, R., Hansson, H. C., Viisanen, Y., Laaksonen, A.,
722 and O'Dowd, C. D.: Overview of the international project on biogenic aerosol formation in the
723 boreal forest (BIOFOR), *Tellus Series B-Chemical and Physical Meteorology*, 53, 324-343,
724 <https://doi.org/10.1034/j.1600-0889.2001.530402.x>, 2001.

725 Kurtén, T., Møller, K. H., Nguyen, T. B., Schwantes, R. H., Misztal, P. K., Su, L., Wennberg, P. O., Fry,
726 J. L., and Kjaergaard, H. G.: Alkoxy radical bond scissions explain the anomalously low secondary
727 organic aerosol and organonitrate yields from α -pinene + NO_3 , *J. Phys. Chem. L*, 8, 2826-2834,
728 <https://doi.org/10.1021/acs.jpcclett.7b01038>, 2017.

729 Lee, B. H., D'Ambro, E. L., Lopez-Hilfiker, F. D., Schobesberger, S., Mohr, C., Zawadowicz, M. A., Liu,
730 J., Shilling, J. E., Hu, W., Palm, B. B., Jimenez, J. L., Hao, L., Virtanen, A., Zhang, H., Goldstein,
731 A. H., Pye, H. O. T., and Thornton, J. A.: Resolving ambient organic aerosol formation and aging
732 pathways with simultaneous molecular composition and volatility observations, *ACS Earth Space*
733 *Chem.*, 4, 391-402, <https://doi.org/10.1021/acsearthspacechem.9b00302>, 2020.

734 Lee, S. H., Uin, J., Guenther, A. B., de Gouw, J. A., Yu, F., Nadykto, A. B., Herb, J., Ng, N. L., Koss, A.,
735 Brune, W. H., Baumann, K., Kanawade, V. P., Keutsch, F. N., Nenes, A., Olsen, K., Goldstein, A.,
736 and Ouyang, Q.: Isoprene suppression of new particle formation: Potential mechanisms and
737 implications, *J. Geophys. Res.-Atmos.*, 121, <https://doi.org/10.1002/2016jd024844>, 2016a.

738 Lee, S. H., Uin, J., Guenther, A. B., de Gouw, J. A., Yu, F. Q., Nadykto, A. B., Herb, J., Ng, N. L., Koss,
739 A., Brune, W. H., Baumann, K., Kanawade, V. P., Keutsch, F. N., Nenes, A., Olsen, K., Goldstein,
740 A., and Ouyang, Q.: Isoprene suppression of new particle formation: Potential mechanisms and
741 implications, *J. Geophys. Res.-Atmos.*, 121, 14621-14635, <https://doi.org/10.1002/2016jd024844>,
742 2016b.

743 Li, D., Huang, W., Wang, D., Wang, M., Thornton, J. A., Caudillo, L., Rörup, B., Marten, R., Scholz, W.,
744 Finkenzeller, H., Marie, G., Baltensperger, U., Bell, D. M., Brasseur, Z., Curtius, J., Dada, L.,
745 Duplissy, J., Gong, X., Hansel, A., He, X.-C., Hofbauer, V., Junninen, H., Krechmer, J. E., Kürten,
746 A., Lamkaddam, H., Lehtipalo, K., Lopez, B., Ma, Y., Mahfouz, N. G. A., Manninen, H. E., Mentler,
747 B., Perrier, S., Petäjä, T., Pfeifer, J., Philippov, M., Schervish, M., Schobesberger, S., Shen, J., Surdu,
748 M., Tomaz, S., Volkamer, R., Wang, X., Weber, S. K., Welti, A., Worsnop, D. R., Wu, Y., Yan, C.,
749 Zauner-Wieczorek, M., Kulmala, M., Kirkby, J., Donahue, N. M., George, C., El-Haddad, I.,
750 Bianchi, F., and Riva, M.: Nitrate radicals suppress biogenic new particle formation from
751 monoterpene oxidation, *Environ. Sci. Technol.*, 58, 1601-1614,
752 <https://doi.org/10.1021/acs.est.3c07958>, 2024.

753 Li, X. X., Chee, S., Hao, J. M., Abbatt, J. P. D., Jiang, J. K., and Smith, J. N.: Relative humidity effect
754 on the formation of highly oxidized molecules and new particles during monoterpene oxidation,

755 Atmos. Chem. Phys., 19, 1555-1570, <https://doi.org/10.5194/acp-19-1555-2019>, 2019.

756 Li, Y., Pöschl, U., and Shiraiwa, M.: Molecular corridors and parameterizations of volatility in the
757 chemical evolution of organic aerosols, Atmos. Chem. Phys., 16, 3327-3344,
758 <https://doi.org/10.5194/acp-16-3327-2016>, 2016.

759 Liebmann, J., Karu, E., Sobanski, N., Schuladen, J., Ehn, M., Schallhart, S., Quéléver, L., Hellen, H.,
760 Hakola, H., Hoffmann, T., Williams, J., Fischer, H., Lelieveld, J., and Crowley, J. N.: Direct
761 measurement of NO₃ radical reactivity in a boreal forest, Atmos. Chem. Phys., 18, 3799-3815,
762 <https://doi.org/10.5194/acp-18-3799-2018>, 2018.

763 Liu, J., D'Ambro, E. L., Lee, B. H., Schobesberger, S., Bell, D. M., Zaveri, R. A., Zelenyuk, A., Thornton,
764 J. A., and Shilling, J. E.: Monoterpene photooxidation in a continuous-flow chamber: SOA yields
765 and impacts of oxidants, NO(x), and VOC precursors, Environ. Sci. Technol., 56, 12066-12076,
766 <https://doi.org/10.1021/acs.est.2c02630>, 2022.

767 Martinez, E., Cabanas, B., Aranda, A., and Martin, P.: Kinetics of the reactions of NO₃ radical with
768 selected monoterpenes: A temperature dependence study, Environ. Sci. Technol., 32, 3730-3734,
769 <https://doi.org/10.1021/es970899t>, 1998.

770 Mentel, T., Springer, M., Ehn, M., Kleist, E., Pullinen, I., Kurtén, T., Rissanen, M., Wahner, A., and Wildt,
771 J.: Formation of highly oxidized multifunctional compounds: autoxidation of peroxy radicals
772 formed in the ozonolysis of alkenes—deduced from structure–product relationships, Atmos. Chem.
773 Phys., 15, 6745-6765, <https://doi.org/10.5194/acp-15-6745-2015>, 2015.

774 Mohr, C., Lopez-Hilfiker, F. D., Yli-Juuti, T., Heitto, A., Lutz, A., Hallquist, M., D'Ambro, E. L.,
775 Rissanen, M. P., Hao, L., Schobesberger, S., Kulmala, M., Mauldin, R. L., Makkonen, U., Sipilä,
776 M., Petäjä, T., and Thornton, J. A.: Ambient observations of dimers from terpene oxidation in the
777 gas phase: Implications for new particle formation and growth, Geophysical Research Letters, 44,
778 2958-2966, [10.1002/2017gl072718](https://doi.org/10.1002/2017gl072718), 2017.

779 Molteni, U., Simon, M., Heinritzi, M., Hoyle, C. R., Bernhammer, A.-K., Bianchi, F., Breitenlechner, M.,
780 Brilke, S., Dias, A., Duplissy, J., Frege, C., Gordon, H., Heyn, C., Jokinen, T., Kürten, A., Lehtipalo,
781 K., Makhmutov, V., Petäjä, T., Pieber, S. M., Praplan, A. P., Schobesberger, S., Steiner, G., Stozhkov,
782 Y., Tomé, A., Tröstl, J., Wagner, A. C., Wagner, R., Williamson, C., Yan, C., Baltensperger, U.,
783 Curtius, J., Donahue, N. M., Hansel, A., Kirkby, J., Kulmala, M., Worsnop, D. R., and Dommen, J.:
784 Formation of highly oxygenated organic molecules from α -pinene ozonolysis: chemical
785 characteristics, mechanism, and kinetic model development, ACS Earth Space Chem., 3, 873-883,
786 <https://doi.org/10.1021/acsearthspacechem.9b00035>, 2019.

787 Mutzel, A., Zhang, Y., Böge, O., Rodigast, M., Kolodziejczyk, A., Wang, X., and Herrmann, H.:
788 Importance of secondary organic aerosol formation of α -pinene, limonene, and m-cresol comparing
789 day- and nighttime radical chemistry, Atmos. Chem. Phys., 21, 8479-8498,
790 <https://doi.org/10.5194/acp-21-8479-2021>, 2021.

791 Newland, M. J., Rickard, A. R., Sherwen, T., Evans, M. J., Vereecken, L., Muñoz, A., Ródenas, M., and
792 Bloss, W. J.: The atmospheric impacts of monoterpene ozonolysis on global stabilised Criegee
793 intermediate budgets and SO₂ oxidation: experiment, theory and modelling, Atmos. Chem. Phys.,
794 18, 6095-6120, <https://doi.org/10.5194/acp-18-6095-2018>, 2018.

795 Nguyen, T. B., Crounse, J. D., Teng, A. P., St. Clair, J. M., Paulot, F., Wolfe, G. M., and Wennberg, P. O.:
796 Rapid deposition of oxidized biogenic compounds to a temperate forest, P. Natl. Acad. Sci. USA,
797 112, <https://doi.org/10.1073/pnas.1418702112>, 2015.

798 Perraud, V., Bruns, E. A., Ezell, M. J., Johnson, S. N., Greaves, J., and Finlayson-Pitts*, B. J.:

799 Identification of organic nitrates in the NO₃ radical initiated oxidation of α -pinene by atmospheric
800 pressure chemical ionization mass spectrometry, *Environ. Sci. Technol.*, 44, 5887–5893,
801 <https://doi.org/10.1021/es1005658>, 2010.

802 Pye, H. O. T., Ward-Caviness, C. K., Murphy, B. N., Appel, K. W., and Seltzer, K. M.: Secondary organic
803 aerosol association with cardiorespiratory disease mortality in the United States, *Nat. Commun.*, 12,
804 <https://doi.org/10.1038/s41467-021-27484-1>, 2021.

805 Schervish, M. and Donahue, N. M.: Peroxy radical chemistry and the volatility basis set, *Atmos. Chem.*
806 *Phys.*, 20, 1183-1199, <https://doi.org/10.5194/acp-20-1183-2020>, 2020.

807 Shen, H., Vereecken, L., Kang, S., Pullinen, I., Fuchs, H., Zhao, D., and Mentel, T. F.: Unexpected
808 significance of a minor reaction pathway in daytime formation of biogenic highly oxygenated
809 organic compounds, *Sci. Adv.*, 8, eabp8702, <https://doi.org/10.1126/sciadv.abp8702>, 2022.

810 Shrivastava, M., Cappa, C. D., Fan, J., Goldstein, A. H., Guenther, A. B., Jimenez, J. L., Kuang, C.,
811 Laskin, A., Martin, S. T., Ng, N. L., Petaja, T., Pierce, J. R., Rasch, P. J., Roldin, P., Seinfeld, J. H.,
812 Shilling, J., Smith, J. N., Thornton, J. A., Volkamer, R., Wang, J., Worsnop, D. R., Zaveri, R. A.,
813 Zelenyuk, A., and Zhang, Q.: Recent advances in understanding secondary organic aerosol:
814 Implications for global climate forcing, *Reviews of Geophysics*, 55, 509-559,
815 [10.1002/2016rg000540](https://doi.org/10.1002/2016rg000540), 2017.

816 Simon, M., Dada, L., Heinritzi, M., Scholz, W., Stolzenburg, D., Fischer, L., Wagner, A. C., Kürten, A.,
817 Rörup, B., He, X.-C., Almeida, J., Baalbaki, R., Baccarini, A., Bauer, P. S., Beck, L., Bergen, A.,
818 Bianchi, F., Bräkling, S., Brilke, S., Caudillo, L., Chen, D., Chu, B., Dias, A., Draper, D. C., Duplissy,
819 J., El-Haddad, I., Finkenzeller, H., Frege, C., Gonzalez-Carracedo, L., Gordon, H., Granzin, M.,
820 Hakala, J., Hofbauer, V., Hoyle, C. R., Kim, C., Kong, W., Lamkaddam, H., Lee, C. P., Lehtipalo,
821 K., Leiminger, M., Mai, H., Manninen, H. E., Marie, G., Marten, R., Mentler, B., Molteni, U.,
822 Nichman, L., Nie, W., Ojdanic, A., Onnela, A., Partoll, E., Petäjä, T., Pfeifer, J., Philippov, M.,
823 Quéléver, L. L. J., Ranjithkumar, A., Rissanen, M. P., Schallhart, S., Schobesberger, S., Schuchmann,
824 S., Shen, J., Sipilä, M., Steiner, G., Stozhkov, Y., Tauber, C., Tham, Y. J., Tomé, A. R., Vazquez-
825 Pufleau, M., Vogel, A. L., Wagner, R., Wang, M., Wang, D. S., Wang, Y., Weber, S. K., Wu, Y., Xiao,
826 M., Yan, C., Ye, P., Ye, Q., Zauner-Wieczorek, M., Zhou, X., Baltensperger, U., Dommen, J., Flagan,
827 R. C., Hansel, A., Kulmala, M., Volkamer, R., Winkler, P. M., Worsnop, D. R., Donahue, N. M.,
828 Kirkby, J., and Curtius, J.: Molecular understanding of new-particle formation from α -pinene
829 between -50 and $+25$ °C, *Atmos. Chem. Phys.*, 20, 9183-9207, [https://doi.org/10.5194/acp-20-](https://doi.org/10.5194/acp-20-9183-2020)
830 [9183-2020](https://doi.org/10.5194/acp-20-9183-2020), 2020.

831 Stone, D., Whalley, L. K., and Heard, D. E.: Tropospheric OH and HO₂ radicals: field measurements and
832 model comparisons, *Chem. Soc. Rev.*, 41, <https://doi.org/10.1039/c2cs35140d>, 2012.

833 Vereecken, L., Novelli, A., and Taraborrelli, D.: Unimolecular decay strongly limits the atmospheric
834 impact of Criegee intermediates, *Phys. Chem. Chem. Phys.*, 19, 31599-31612,
835 <https://doi.org/10.1039/c7cp05541b>, 2017.

836 Wang, Y., Zhao, Y., Li, Z., Li, C., Yan, N., and Xiao, H.: Importance of hydroxyl radical chemistry in
837 isoprene suppression of particle formation from α -pinene ozonolysis, *ACS Earth Space Chem.*, 5,
838 487-499, <https://doi.org/10.1021/acsearthspacechem.0c00294>, 2021.

839 Wolfe, G. M., Marvin, M. R., Roberts, S. J., Travis, K. R., and Liao, J.: The framework for 0-D
840 atmospheric modeling (F0AM) v3. 1, *Geosci. Model Dev.*, 9, 3309-3319,
841 <https://doi.org/10.5194/gmd-9-3309-2016>, 2016.

842 Xu, L., Møller, K. H., Crounse, J. D., Otkjær, R. V., Kjaergaard, H. G., and Wennberg, P. O.:

843 Unimolecular reactions of peroxy radicals formed in the oxidation of α -pinene and β -pinene by
844 hydroxyl radicals, *J. Phys. Chem. A*, 123, 1661-1674, <https://doi.org/10.1021/acs.jpca.8b11726>,
845 2019.

846 Zang, H., Huang, D., Zhong, J., Li, Z., Li, C., Xiao, H., and Zhao, Y.: Direct probing of acylperoxy
847 radicals during ozonolysis of α -pinene: constraints on radical chemistry and production of highly
848 oxygenated organic molecules, *Atmos. Chem. Phys.*, 23, 12691-12705, [https://doi.org/10.5194/acp-](https://doi.org/10.5194/acp-23-12691-2023)
849 23-12691-2023, 2023.

850 Zhang, H., Yee, L. D., Lee, B. H., Curtis, M. P., Worton, D. R., Isaacman-VanWertz, G., Offenberg, J. H.,
851 Lewandowski, M., Kleindienst, T. E., Beaver, M. R., Holder, A. L., Lonneman, W. A., Docherty, K.
852 S., Jaoui, M., Pye, H. O. T., Hu, W., Day, D. A., Campuzano-Jost, P., Jimenez, J. L., Guo, H., Weber,
853 R. J., de Gouw, J., Koss, A. R., Edgerton, E. S., Brune, W., Mohr, C., Lopez-Hilfiker, F. D., Lutz,
854 A., Kreisberg, N. M., Spielman, S. R., Hering, S. V., Wilson, K. R., Thornton, J. A., and Goldstein,
855 A. H.: Monoterpenes are the largest source of summertime organic aerosol in the southeastern
856 United States, *P. Natl. Acad. Sci. USA*, 115, 2038-2043, <https://doi.org/10.1073/pnas.1717513115>,
857 2018.

858 Zhang, X., McVay, R. C., Huang, D. D., Dalleska, N. F., Aumont, B., Flagan, R. C., and Seinfeld, J. H.:
859 Formation and evolution of molecular products in α -pinene secondary organic aerosol, *P. Natl. Acad.*
860 *Sci. USA*, 112, 14168-14173, <https://doi.org/10.1073/pnas.1517742112>, 2015.

861 Zhang, Y., Peräkylä, O., Yan, C., Heikkinen, L., Äijälä, M., Daellenbach, K. R., Zha, Q., Riva, M.,
862 Garmash, O., Junninen, H., Paatero, P., Worsnop, D., and Ehn, M.: Insights into atmospheric
863 oxidation processes by performing factor analyses on subranges of mass spectra, *Atmos. Chem.*
864 *Phys.*, 20, 5945-5961, <https://doi.org/10.5194/acp-20-5945-2020>, 2020.

865 Zhao, Y., Thornton, J. A., and Pye, H. O. T.: Quantitative constraints on autoxidation and dimer formation
866 from direct probing of monoterpene-derived peroxy radical chemistry, *P. Natl. Acad. Sci. USA*, 115,
867 12142-12147, <https://doi.org/10.1073/pnas.1812147115>, 2018.

868 Zhao, Y., Yao, M., Wang, Y., Li, Z., Wang, S., Li, C., and Xiao, H.: Acylperoxy radicals as key
869 intermediates in the formation of dimeric compounds in α -pinene secondary organic aerosol,
870 *Environ. Sci. Technol.*, 56, 14249-14261, <https://doi.org/10.1021/acs.est.2c02090>, 2022.

871 Zhao, Z., Zhang, W., Alexander, T., Zhang, X., Martin, D. B. C., and Zhang, H.: Isolating alpha-pinene
872 ozonolysis pathways reveals new insights into peroxy radical chemistry and secondary organic
873 aerosol formation, *Environ. Sci. Technol.*, 55, 6700-6709, <https://doi.org/10.1021/acs.est.1c02107>,
874 2021.

875